2-P

ELEVATED TEMPERATURE DEFORMATION OF THORIA DISPERSED NICKEL-CHROMIUM

by

R. D. Kane and L. J. Ebert

ANNUAL STATUS REPORT

June 1974

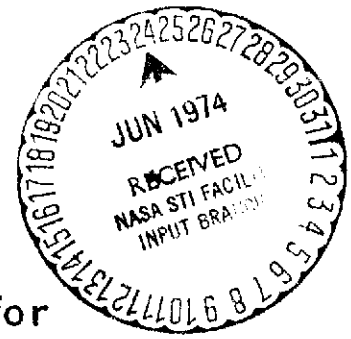

Prepared for

NATIONAL AERONAUTICS AND SPACE ADMINISTRATION

Grant NGR 36-003-094

School of Engineering

Department of Metallurgy and Materials Science

Case Western Reserve University

Cleveland, Ohio 44106

106

ELEVATED TEMPERATURE DEFORMATION OF THORIA DISPERSED NICKEL-CHROMIUM

by

R. D. Kane and L. J. Ebert

ANNUAL STATUS REPORT

June 1974

Prepared for

NATIONAL AERONAUTICS AND SPACE ADMINISTRATION

Grant NGR 36-003-094

School of Engineering

Department of Metallurgy and Materials Science

Case Western Reserve University

Cleveland, Ohio 44106

ELEVATED TEMPERATURE DEFORMATION OF THORIA DISPERSED NICKEL-CHROMIUM

NGR 36-003-094

ANNUAL STATUS REPORT

June 1974

Prepared by R. D. Kane and L. J. Ebert

Submitted to:

Office of Grants and Research Grants

Attention Code SC

National Aeronautics and Space Administration

Washington, D. C. 20546

School of Engineering
Department of Metallurgy and Materials Science
Case Western Reserve University
Cleveland, Ohio 44106

ELEVATED TEMPERATURE DEFORMATION OF

THORIA DISPERSED NICKEL-CHROMIUM

Abstract

by

RUSSELL DEAN KANE

The deformation behavior of thoria dispersed nickel-chromium (TD-NiCr) was examined over the temperature range 593°C (1100°F) to 1260°C (2300°F) in tension and compression and at 1093°C (2000°F) in creep. Major emphasis was placed on 1) the effects of the material and test related variables (grain size, temperature, stress and strain rate) on the deformation process, and 2) the evaluation of single crystal TD-NiCr material produced by a directional recrystallization process. Elevated temperature yield strength levels and creep activation enthalpies were found to increase with increasing grain size reaching maximum values for the single crystal TD-NiCr. Stress exponent of the steady state creep rate was also significantly higher for the single crystal TD-NiCr as compared to that determined for the polycrystalline materials.

The elevated temperature deformation of TD-NiCr was analyzed in terms of two concurrent - parallel processes: diffusion controlled grain boundary sliding, and dislocation motion. The characteristics of the dislocation motion deformation mode (as observed in the single crystal)

suggest that dislocation motion is strongly affected by dislocation-particle interactions arising from surface tension stresses around thoria particles. The relative contribution of dislocation motion and grain boundary sliding in TD-NiCr was estimated. In creep, grain boundary sliding was found to predominate for the small, equiaxed grain structures, whereas the dislocation deformation mode became significant only for the large grain TD-NiCr (at relatively high creep stresses) and the single crystal material.

FOREWORD

This Annual Status Report describes investigations conducted under NASA Grant NGR 36-003-094 over the period June 1973 to June 1974. This report describes the work presented to Case Western Reserve University by Russell D. Kane in partial fulfillment of the requirements for the degree of Doctor of Philosophy in Metallurgy and Materials Science.

TABLE OF CONTENTS

TABLE OF CONTENTS (Continued)

LIST OF FIGURES

LIST OF FIGURES (Continued)

LIST OF FIGURES (Continued)

LIST OF TABLES

CHAPTER I

INTRODUCTION

Dispersion strengthened alloys are those which derive their mechanical properties from a uniform dispersion of sub-micron size second-phase particles in a metallic matrix of reasonably good high temperature properties. Characteristically, these materials retain a significant portion of their ambient temperature strength at elevated temperatures. Therefore, dispersion strengthening has proved to be extremely promising in the development of materials for applications demanding relatively high strength and dependability at high temperatures.

The first generation of engineeringly significant dispersion strengthened materials were those which contained a uniform dispersion of thoria (ThO_2) particles in a commercially pure nickel matrix, i.e. TD-Nickel. Thoria was chosen as the dispersed phase because of its chemical inertness and mechanical stability in the nickel matrix at anticipated use temperatures. While the dispersion strengthening characteristics of the thoria successfully increased the temperature range of usable strengths of nickel up to 1316°C (2400°F), the poor oxidation resistance of nickel at these temperatures seriously limited the engineering application of TD-Nickel.

Consequently, research efforts were directed to the development of a "second generation" of thoria dispersed alloys which were intended to overcome the deficiencies of TD-Nickel. The result of this series of developments was thoria dispersed nickel-chromium

(TD-NiCr). This alloy was designed to use the dispersion strengthening properties of the thoria, the high melting point of the nickel-chromium matrix, and the high temperature oxidation resistance imparted to this alloy by the addition of the chromium.

Purpose of the Present Investigation

In recent years much has been learned of the elevated temperature deformation mechanisms of TD-Nickel, the predecessor of TD-NiCr. However, due to the recentness of the development of TD-NiCr, relatively little research[4,5,6,7,11] has been performed to evaluate this material in light of the work that has been done on TD-Nickel. More importantly, little effort has been placed on the determination of the basic factors which produce the elevated temperature mechanical properties of TD-NiCr and the manner in which these factors can be controlled. As shown for TD-Nickel[2,3], only through such investigations can the optimization of high temperature use of TD-NiCr materials be achieved.

Research performed on TD-Nickel[1,2,3,6] has indicated that the elevated temperature tensile and creep properties of this material are strongly dependent on material-related variables, i.e. grain size and shape. It was found that insight into the basic deformation mechanisms operative in TD-Nickel could be attained by examining the effects of these material variables on the elevated temperature mechanical properties. Because of the inherent similarities of TD-Nickel and TD-NiCr, it was felt that a similar

study would be equally important for TD-NiCr.

The purpose of the present study was one of examining the mechanical behavioral characteristics of TD-NiCr materials at elevated temperatures in order to gain a more basic understanding of the deformation processes occurring in TD-NiCr and in dispersion strengthened materials in general. The major effort was placed in determining the effects of the material variables (i.e. grain size) on the mechanical properties of TD-NiCr in tensile, compression and creep loading situations. Emphasis was placed on the analysis of the thermodynamic parameters which describe the deformation process, i.e. activation enthalpy, and the correlation of these parameters to the theoretical and phenomenalogical aspects of the deformation process.

CHAPTER II

ELEVATED TEMPERATURE DEFORMATION OF TD-NiCr ALLOYS

Upon surveying the literature regarding the elevated temperature deformation of TD-NiCr alloys[4-7,11], it is immediately obvious that relatively little work has been performed when compared to that published on TD-nickel. In this section, the literature available on TD-NiCr will be reviewed and discussed. All investigations cited are concerned with the behavior of TD-NiCr above one-half its absolute melting temperature.

Tensile Properties

In TD-NiCr the elevated temperature yield and tensile strength levels and ductility have been shown to be very sensitive to grain size[4,5]. Both yield and tensile strength increase with increasing grain size. It has been reported that after an initial large increase in strength level with grain size in the small grain size region, only a moderate increase in strength level is observed for further increases in grain size[4] at a given temperature. Because of the tendency for TD-NiCr alloys to recrystallize in nearly equiaxed grain shapes (Length-to-Diameter, or L/D ratios approaching unity), the effects of grain shape on the elevated temperature mechanical properties have only been studied to a limited degree[6]. In the range of L/D ratios from 1 to 8, the

yield strength of TD-NiCr increases linearly with increasing L/D ratio. Anisotropy of strength properties results from grain anisotropy[5]. Strength levels decrease as the axis of testing departs from the direction of grain elongation (which is usually the processing direction).

Ductility varies inversely as strength with respect to changes in the grain size. Fine grained TD-NiCr of nearly equixed shape had the greatest ductility, but minimal strength. The ductility decreased dramatically with increasing grain size.

No mention of activation enthalpy measurements made during tensile tests appear in the literature.

Creep Properties

The bulk of the data generated thus far concerning the creep behavior of TD-NiCr comes from Wilcox and Clauer[6,7]. Various TD-NiCr alloys have been investigated containing from 0 to 33.7 weight percent chromium and approximately 1 volume percent thoria. (The materials investigated had a grain size of approximately 0.02mm and L/D=1-2). It was observed that the resistance to creep deformation in these alloys increased with increasing amounts of chromium. The phenomenological creep expression that describes the stress and temperature dependence of the steady state creep rate, $\dot{\varepsilon}$, was found to be

$$\dot{\varepsilon} = K\left(\frac{\sigma}{E}\right)^n \exp(-Q_c/RT) \qquad \ldots\ldots(1)$$

where K = constant, σ = applied stress, E = elastic modulus, n = stress exponent, R = gas constant, T = absolute temperature, and Q_c = activation enthalpy for creep. Similar expressions have also been used to describe the creep behavior of TD-Nickel[8,9].

Using the expression given above, stress exponents of approximately 7 and activation enthalpies of 2.8 to 3.2 ev. were reported. The stress exponent was found to be insensitive to composition whereas the activation enthalpy increased with increasing chromium concentration and was very close to the self-diffusion enthalpy. No attempt was made to determine the effects of stress or grain size on the values of these parameters.

Similar data reported for TD-Nickel[8,9] show that TD-Nickel with a grain size of ~0.05mm and L/D ~1 have values very similar to those found for TD-NiCr (n = 7 and Q_c = 2.78 ev.). However, for materials conditions of TD-Nickel having a grain size of 0.001mm and L/D = 15-20, values of the stress exponent, n, were near 40 and the activation enthalpy, Q_c, was 8.25 ev. There has been no mention of similarly high values of stress exponent and activation enthalpy for any TD-NiCr alloys.

The work of Wilcox and Clauer[7] on TD-NiCr alloys as well as work on non-thoriated nickel-chromium alloys[10] noted that the addition of chromium into pure nickel has a great effect on the stacking fault energy (SFE). The SFE of pure nickel has been reported to be between 240 to 415 ergs/cm^2 decreasing to a value of 42-80 ergs/cm^2 with the addition of 20 weight percent chromium.

Accompanying this decrease in SFE was a corresponding decrease in the steady state creep rate, $\dot{\varepsilon}$. The expression used by Wilcox and Clauer to describe this dependence was

$$\dot{\varepsilon}_s = C\gamma^m(\sigma/E)^n D \qquad \ldots\ldots(2)$$

where C = constant, γ = stacking fault energy, m = the stacking fault energy exponent and D = the chemical self-diffusivity.

CHAPTER III

THEORY OF ELEVATED TEMPERATURE DEFORMATION OF DISPERSION STRENGTHENED MATERIALS

Deformation theories of dispersion strengthened materials can be classified into three categories: 1) dislocation models, 2) grain boundary sliding models, and 3) concurrent process models. Concurrent process models are those which attempt to describe the deformation process in terms of the relative contributions of dislocation motion and grain boundary sliding. A review of the dislocation and grain boundary sliding models has been presented by Petrovic[3]; therefore, these will be considered only briefly. Major emphasis will be placed on the description of the concurrent process models.

Dislocation Models

The initial attempt at describing the steady state creep behavior of dispersion strengthened materials was proposed by Ansell and Weertman[12]. Assuming that the rate controlling mechanism was the climb of dislocations over second-phase particles, two expressions were presented.

(Low Stresses) $$\dot{\gamma}_s = \frac{A\tau}{R_o^2} \exp(-Q_{sd}/kT) \quad \ldots\ldots(3)$$

(Intermediate Stresses) $$\dot{\gamma}_s = \frac{A\tau d^2}{R_o G^3 T} \exp(-Q_{sd}/kT) \quad \ldots\ldots(4)$$

where $\dot{\gamma}_s$ = shear strain rate during steady state creep, A = constant, R_o = particle radius, τ = shear stress, G = shear modulus, d = interparticle spacing, Q_{sd} = the self-diffusion enthalpy, k = Boltzman constant and T = absolute temperature. Further analysis of the dislocation climb model was given by Wilcox and Clauer[13]. A similar expression was proposed with the only difference arising in the pre-exponential stress term which results from the assumption that the mobile dislocation density was stress dependent.

Various other attempts have been made to explain the creep behavior of dispersion strengthened materials using dislocation models[14-17]. These theories are of limited use because of their extreme dependence on the formation of very specific types of dislocation substructures or because they do not consider other processes occurring at elevated temperatures. More importantly, dislocation models, in the broad sense, cannot describe the large grain size and shape sensitivities observed in the elevated temperature deformation of dispersion strengthened materials.

Grain Boundary Sliding Models

The first model proposed to describe the elevated temperature deformation of dispersion strengthened materials which incorporated grain boundary effects was presented by Fraser and Evans[18]. It was presumed that the main function of the dispersed phase was that of increasing the load carrying capability of the material

within the grains relative to the grain boundary surface area. The mechanism by which this occurred was the impediment of dislocation motion within the grains. In describing this situation, a fiber composite approach was used whereby each grain was considered a fiber strengthened by the presence of the second phase. Since applied loads must be transferred across grain boundaries, the total strength of this material depends on the relative strengths of the grain and the grain boundary regions. Consequently, at temperatures above the equi-cohesive point (usually above half the absolute melting temperature) where the grain boundaries are weaker than the grains, the grain boundary effects will determine the total strength.

Using the approach stated above, it was proposed that the material will tend to deform by grain boundary processes (i.e. grain boundary sliding) unless the grain boundary surface area experiencing the applied stress is increased to a point where its load carrying capability is greater than or equal to that of the grain interior. The significance of this proposal is that it would be possible to make materials more resistant to elevated temperature deformation by increasing their grain size or by increasing the L/D ratio.

Raj and Ashby[19] have presented a theoretical description of grain boundary sliding with diffusional accommodation. Deformation processes such as these are expected to occur when the combination of low stresses and temperatures above one-half the

absolute melting point are present (i.e. creep conditions). The proposed expression for the steady state creep rate was:

$$\dot{\gamma}_s = \frac{A\tau}{g^2(L/D)^a} \exp(-Q_{sd}/kT) \quad \ldots\ldots(5)$$

where g = the grain diameter, and a = 2 for ordinary values of L/D. When L/D values are large, a = 1.

The effect of the dispersed phase particles on grain boundary sliding processes was also considered; the particles were predicted to have only a slight effect on reducing the grain boundary sliding rate. However, it was suggested by Ashby[20] that dispersed particles could affect the ability of grain boundaries to emit or absorb vacancies, thus influencing the grain boundary sliding characteristics.

Concurrent Process Model

It is apparent that neither dislocation models nor grain boundary sliding models can explain the characteristics of the elevated temperature deformation of dispersion strengthened materials. Dislocation models do not predict the extreme grain size and shape sensitivities, and grain boundary sliding models fail to show the role of the particle dispersion in improving the elevated temperature deformation resistance. Furthermore, none of these proposed theories can account for the high activation enthalpies and stress sensitivities observed in some cases for dispersion strengthened materials.

It has been proposed[3,21] that two concurrent (parallel) processes may contribute to the elevated temperature deformation of polycrystalline dispersion strengthened materials. These processes are 1) dislocation motion and 2) diffusion controlled grain boundary sliding. From such an analysis it has been suggested[3,21] that the steady state creep rate, $\dot{\gamma}_s$, will have the form

$$\dot{\gamma}_s = \dot{\gamma}_{DIS} + \dot{\gamma}_{GBS} \qquad \ldots\ldots(6)$$

where $\dot{\gamma}_{DIS}$ = shear strain rate arising from dislocation motion and $\dot{\gamma}_{GBS}$ = shear strain rate from diffusion controlled grain boundary sliding. The relative contribution of both of these mechanisms will determine the overall creep rate observed in the material.

The form of the shear strain rate terms arising from dislocation motion and grain boundary sliding was examined by Petrovic and Ebert[3,21] in order to explain the elevated temperature deformation characteristics of TD-Nickel. It was proposed that both dislocation glide and climb processes are affected by stresses in the matrix around small, incoherent second-phase particles. These stresses are attributable to surface tension effects acting at the particle-matrix interface. In essence, the particle produces a stable "hole" in the metal matrix of an extremely small size.

It was shown that if the matrix is assumed to be an infinite, isotropic solid, the following stresses were developed around the particles:

$$\sigma_{RR} = \frac{2E_s}{R_o} (R_o/R)^3 \qquad \ldots\ldots (7a)$$

$$\sigma_{\theta\theta} = \sigma_{\phi\phi} = -1/2\ \sigma_{RR} \qquad \ldots\ldots (7b)$$

where σ_{RR} = radial stress, $\sigma_{\theta\theta} = \sigma_{\phi\phi}$ = circumferential stresses, E_s = the surface energy, R_o = the particle radius, and R = the radial distance from the particle. A triaxial stress state results which is totally deviational in character. It was determined that these surface tension stresses tend to interact significantly with matrix dislocations creating both glide and climb "pinning" forces which impede the motion of the dislocations.

For TD-Nickel, the dislocation-particle interactions described above are not negligible. Interaction energies given by $2R_oE_sb$ (b = Burgers vector) were calculated to be 19.4 ev, whereas the self-diffusion enthalpy of nickel is near 3 ev.

From this analysis it was possible to derive expressions for the shear strain rate resulting from dislocation motion when either dislocation glide or climb is the rate controlling process. Considering dislocation glide to be rate-controlling,

$$\dot{\gamma}_{DIS} = \frac{\pi\rho b\nu d}{2} \exp\ (-\Delta H/kT) \qquad \ldots\ldots (8)$$

represents the shear strain rate for dislocation motion where ρ = the mobile dislocation density and ν = frequency of vibration of the dislocation segment involved in thermal activation. The value of ΔH in this expression can be estimated to be 19.4 ev. for

TD-Nickel. Similarly, considering dislocation climb to be rate-controlling, the shear strain rate attributable to dislocation motion can be represented by

$$\dot{\gamma}_{DIS} = \frac{\rho d\, D_o \Omega}{a R_o kT} (\tau - \tau_i^c) \exp(-Q_{sd}/kT) \quad \ldots\ldots (9)$$

where D_o = diffusion coefficient pre-exponential term, Ω = the atomic volume, τ_i^c = internal stress below which climb of dislocations over dispersed phase particles will not occur ($\tau_i^c = ME_s/R_o$ where $M \leq 1$) and Q_{sd} = the self-diffusion enthalpy.

Using the expression for the shear strain rate from grain boundary sliding derived by Raj and Ashby[19], shown in equation (5), the expression for the total shear strain rate can be attained by combining it with the appropriate expression for dislocation motion (equation 8 or 9) as shown in equation 6. This expression (assuming dislocation glide is rate-controlling) for the total shear strain rate was shown to predict not only the high activation enthalpies and stress sensitivities observed for TD-Nickel but it also takes into account the grain size and shape dependencies of the elevated temperature mechanical properties.

CHAPTER IV

MATERIALS AND PROCEDURES

Materials

TD-Nickel-Chromium (TD-NiCr), supplied by the Fansteel Corporation in the form of 0.1 inch thick sheet, was used for the majority of this study. This material is characteristically a single phase, nickel + 20 weight percent chromium alloy containing approximately 2 volume percent thoria (ThO_2) as the dispersed phase. Powder metallurgical techniques are employed in the fabrication of this material. Thoria containing nickel-chromium powder is consolidated, then sintered and hot rolled in the temperature range 1093-1149°C (2000-2100°F). The final reduction is performed by warm rolling at 704°C (1300°F).

The chemical analysis of the TD-NiCr sheet material examined is shown in Table I. This material was received in the unannealed form containing a partially recovered substructure with grains less than 0.001mm in size. Wilcox and Clauer[6] have measured values of 176Å for the thoria particle diameter and 1595Å for the interparticle spacing for TD-NiCr alloys of similar thoria content produced by the Fansteel Corporation.

TD-NiCr was also obtained in a directionally recrystallized form from Dr. R. E. Allen at General Electric Powder Metallurgical Alloys Division. The processing techniques developed by Dr. Allen[22], which involve the annealing of TD-NiCr by the passage of a

steep thermal gradient, produce extremely large and elongated grain structures. A bi-crystal of TD-NiCr produced by this process was supplied with the approximate dimensions of 3" long, 1-1/4" wide and 7/16" deep. The grains and their relative orientations were as shown in Figure 1.

Grain Size Control

It was shown in a previous investigation[4,23] that the grain size (and grain shape to a certain extent) of TD-NiCr 0.1 inch thick sheet could be predictably controlled using selected cyclic cold rolling and annealing treatments. Table II indicates the techniques used to produce the material conditions used in the present study.

A large grain size (Material B, 0.19mm average grain dimension) was produced by annealing the as-received 0.1 inch sheet for 1 hour at 1316°C (2400°F) in argon. Upon transverse cold rolling and subsequent annealing of Material B, grain refinement was observed. An intermediate grain size material (Material L, 0.0086mm average grain dimension) and a fine grain size material (Material D, 0.0037mm average grain dimension) were obtained by respectively cold rolling Material B to reductions of 22 and 48% followed by an annealing treatment of 1316°C (2400°F) for 1 hour in argon. The L/D ratios (Length-to-Thickness dimension) for all of these TD-NiCr materials were between 2-4.

Metallography and Grain Size Measurements

During the previous investigation, no existing grain boundary etching techniques were found satisfactory in revealing the microstructure of TD-NiCr sheet. It was noted that differences in etching behavior were observed depending on specimen orientation. Etching to delineate grain boundaries in this material was also particularly difficult because of the abundance of anneal twins found in the microstructures.

Initially, an electro-chemical etch was developed which delineated the grain boundaries in TD-NiCr sheet. This etch consisted of 6 parts ethanol, 1 part H_2SO_4 and 21 parts H_2O and was used at an etching voltage of 5 volts. However, the efficiency of this etch decreased with increasing grain size.

It was later found that a thermal-oxidation etch provided better grain boundary detail and excellent etching behavior over the entire range of grain sizes produced in this study. This etch consisted of placing metallographically polished specimens in a preheated furnace (air atmosphere). A selective oxidation of the grain boundaries occurred at 593°C (1100°F) for all grain sizes. It was also observed that the larger grain size materials had a tendency to undergo heat tinting of the polished grain surfaces which aided the distinction between grains. Etching times for this procedure were usually in the range of 2-5 minutes depending on the size of the specimen and the grain size; longer times were used for larger grain sizes and specimen sizes. No microstructural

changes were observed as a result of the thermal etching treatment.

The grain sizes of the various TD-NiCr materials were determined by observing the etched microstructures and employing the quantitative metallographic techniques indicated by DeHoff and Rhines[24]. Basically, a line intercept method was used to determine the average grain dimension in each of the following mutually perpendicular directions: 1) rolling direction, 2) rolling plane transverse direction and 3) thickness plane transverse direction. The number of grains per unit volume, N_v, was statistically determined as shown,

$$N_v = 0.7(N_R)(N_{RT})(N_{TT}) \qquad \ldots\ldots(10)$$

where N_R = number of grains/mm in the rolling direction, N_{RT} = number of grains/mm in the rolling plane transverse direction and N_{TT} = number of grains/mm in the thickness plane transverse direction. From N_v the average grain dimension (AGD) was calculated

$$AGD = (0.422/N_v)^{1/3} \qquad \ldots\ldots(11)$$

Table II shows the average grain dimensions for Materials B, L and D. Also indicated are the standard errors about these mean values which represent a 95% confidence level of the grain size data.

Single Crystal TD-NiCr

Single crystal specimens were prepared from the bi-crystal of TD-NiCr provided by Dr. Allen. At the outset, the bi-crystal was macro-etched using a grain contrast etch (40 ml HCl, 60 ml H_2O, 20 gm ferric chloride) and the orientation of the large columnar grains checked using a Laue X-ray back-reflection camera (operating conditions, Tungsten radiation, 20 KV, 40 ma.). The long dimension of the two grains were both [001] crystallographic directions with a relative rotation between grains of 12 degrees about this axis. Both the etching and the Laue photographs revealed a low angle boundary structure within these large grains. Analysis of the Laue spots indicated that the misorientation across the low angle boundaries was 0-2 degrees.

Two types of specimens were cut from the TD-NiCr bi-crystals: 1) single crystal compression blocks and 2) single crystal tensile creep specimens. The compression blocks were of the approximate dimensions 1/8" x 1/8" x 1/4" with a height-to-width ratio of 2:1 or slightly larger (see Figure 2). Specimens of this type were cut from the bulk material using a precision cut-off wheel. Specimen faces were ground using a special fixture insuring the perpendicularity of adjacent surfaces. Because of the small size of these specimens, it was possible to cut them with various crystallographic orientations parallel to the height dimension. Laue photographs were used to check specimen orientations.

The single crystal tensile creep specimens are also shown in Figure 2. The orientation of the tensile axis in these specimens was limited to that of the long dimension of the bi-crystal, i.e. [001].

Elevated Temperature Tensile and Compression Testing

In the previous investigation[4,23] the tensile properties of TD-NiCr sheet (0.2% offset yield strength, tensile strength and ductility) had been investigated as a function of grain size in the temperature range 593°C (1100°F) (0.52 Tm) and 1093°C (2000°F) (0.82 Tm). Therefore, the major emphasis was placed on the generation of data which could be used to determine the thermal activation parameters (i.e. activation enthalpy) for TD-NiCr under normal tensile and compression testing strain rates (0.02-0.2/ minute).

The specimen design used to examine the polycrystalline TD-NiCr materials (Materials B, L and D) is shown in Figure 2. Generous radii of curvature at the specimen shoulders were employed to minimize the frequency of shoulder breaks. The specimen grips used in testing were made of TD-Nickel and designed to undergo no deformation. The grips were lightly oxidized in air at 1093°C (2000°F) for 1 hour prior to testing to eliminate diffusion bonding of the grip section and the specimen.

In order to test the compression blocks (see Figure 2) of the single crystal material, tungsten rams were used to apply the

compressive load. Specimens were tested with and without TD-NiCr pads between the specimen and the tungsten rams with no apparent differences in the recorded data. A boron nitride powder was used to lubricate the end surfaces of the compression blocks.

The test apparatus used to perform the tensile and compression tests was an Instron-Brew furnace combination. Tests were run in the temperature range 593°C (1100°F) to 1260°C (2300°F) under vacuum conditions of 5×10^{-5} torr. Temperature was controlled to ±2.8°C (±5°F) using a Tungsten-5% Rhenium-Tungsten-26% Rhenium thermocouple located at the center of the specimen.

The 0.2% offset yield strength of all of the TD-NiCr materials was measured as a function of testing temperature. Stress relaxation tests were conducted by stopping the machine cross-head at a constant value of strain following yielding and measuring the stress decay with time.

Differential strain rate tests were also performed. These tests consisted of changing the strain rate discontinuously at a point in the plastic flow curve and observing the resultant change in flow stress. The two strain rates used were 0.02/minute and 0.2/minute.

Because of the inherent brittle nature of Material B under usual tensile testing strain rates (elongation 0-1%), it was not possible to conduct relaxation and differential strain rate tests in the tensile deformation mode on this material condition. Therefore, these tests were performed on Materials L and D in tension

and in compression for Material B and the single crystal material.

Elevated Temperature Creep Testing

All creep testing of the polycrystalline TD-NiCr materials was performed in tension using the same specimen and grip designs indicated for elevated temperature tensile testing. Creep tests were performed on Satec creep units equipped with furnace retort assemblies allowing the testing to be run in an inert argon atmosphere. Specimens were loaded using a constant stress lever arm modification similar to that shown by Fullman[25]. The testing temperature for all creep runs was 1093°C (2000°F). Specimen strain measurements were obtained using an LVDT which monitored the motion of the load train above the specimen and displayed the elongation as a function of time on a chart recorder.

Conventional creep tests were performed as a function of applied stress for all three polycrystalline TD-NiCr materials. The data of primary interest were: 1) time to failure (rupture time), 2) steady state creep rate and 3) steady state creep strain.

The thermal activation parameters (i.e. activation enthalpies) were investigated as a function of applied stress, strain and grain size. Differential temperature tests were employed whereby during the creep test, the temperature was changed and upon the restabilization of the temperature, the change in strain rate was measured. Temperature changes were in the range 41.6-44.4°C (75-80°F).

A similar creep testing program was undertaken for the single crystal TD-NiCr material (tensile axis, [001]). Using grip modifications and the compact single crystal creep specimens (see Figure 2c), tests were run at 1093°C (2000°F). Both conventional and differential creep testing was performed. Activation enthalpy determinations were also made.

Scanning Electron Microscopy

Tensile test fracture surfaces were examined with the scanning electron microscope to aid in the characterization of the failure modes. Specimens of Material D tested at 25°C (77°F) and at 1093°C (2000°F) were used in this part of the investigation.

CHAPTER V

RESULTS

Tensile Testing

Typical stress-strain curves for the TD-NiCr materials with the two grain size extremes (Materials B and D, AGD = 0.19mm and 0.0037mm, respectively) are shown in Figure 3 for tensile deformation. In this case the test temperature was 1093°C (2000°F). The 0.2% offset yield strengths of the polycrystalline TD-NiCr (Materials B, L and D) are represented in Figure 4 as a function of temperature.

It was observed that the stress levels for yielding of Materials B, L and D were very temperature dependent, i.e. decreasing with increasing temperature. Yield strengths were also observed to increase with increasing grain size at temperatures above 593°C (1100°F). The extreme grain size dependence of the ductility found in the elevated temperature deformation of TD-NiCr is evident from Figure 3. At 1093°C (2000°F) the ductility increased with decreasing grain size. The brittle behavior of Material B shown in Figure 3 demonstrates the previously-noted necessity for compression testing in the determination of the thermal activation parameters of this large grain material.

Compression Testing

In order to analyze the crystallographic nature of the defor-

mation in single crystal TD-NiCr at elevated temperature, slip lines observed on the surface of deformed specimens were used as the analytical tool. Figure 5a shows the slip lines found after approximately 3% plastic deformation of a TD-NiCr single crystal oriented so that the compression axis was near the center of the standard triangle (i.e. ~321). The slip lines appear as short wavy segments separated by slip-line-free regions. After further compressive deformation, the orientation of the slip plane with respect to the loading axis was determined as shown in Figure 5b. The angle between the slip plane and loading axis was measured to be 44 degrees which corresponds to a classical (111) type slip plane found in face-centered cubic metals[26] (see Figure 6).

Both engineering stress-strain curves and shear stress-shear strain curves were determined from load-elongation data recorded for TD-NiCr single crystals of various orientations. Since the crystallographic nature of the deformation in TD-NiCr single crystals appeared to be similar to that found in non-thoriated face-centered-cubic metals, shear stress and shear strain curves were determined for both single and double glide conditions using expressions derived by Bowen and Christian[29]. The expressions for shear stress, τ, and shear strain, γ, in compression are as follows:

Eqn. 12 for Double Glide: for single glide, see ref. 29

$$\tau = \frac{L}{A_o}\,\frac{1}{l_o}\,\frac{1}{\sqrt{3}}\cos\beta\cos(45°-\beta) \qquad .....(12a)$$

$$\gamma = \sqrt{6}\,\ln\frac{1+\cot\beta}{1+\cot\beta_o} \qquad .....(12b)$$

where A_o = initial cross-sectional area, and l_o = initial specimen length. The value β is the instantaneous angle between the loading axis and active slip direction. For double glide, this is the angle between the loading axis and $\underline{w}$, where $\underline{w}$ is the vector sum of the two operating slip directions. β_o represents the initial angle before testing.

Figure 7 shows the engineering stress-strain curves observed for TD-NiCr single crystal oriented for single glide (i.e. ~<321>) at room temperature (25°C (77°F)), 593°C (1100°F) and 1093°C (2000°F). Similarly, the shear stress - shear strain curves for these tests are shown in Figure 8. Like the polycrystalline TD-NiCr, the single crystal material showed a strong temperature dependence of its yield strength. Figures 7 and 8 indicate that the strain hardening behavior of the single crystal TD-NiCr was also temperature dependent. At room temperature a very high hardening rate was observed; at 593°C (1100°F) a "three stage" type strain hardening behavior prevailed. For deformation at 1093°C (2000°F) virtually no strain hardening was observed for this orientation. An increased strain hardening rate and a slightly higher yield stress were found for crystals oriented for double glide.

The temperature dependence of the yield strength of single crystal TD-NiCr oriented for double glide (i.e. ~<110>) is represented in Figure 9. Also shown in this figure are similar data for Material B, determined in compression. This data for Material B are slightly higher at elevated temperatures than those measured

for this material condition tested in tension (see Figure 4). This effect is probably due to the geometry of the compression specimen and the end constraint effects of this type of test. More importantly, it can be seen that the yield strengths of Material B (0.19mm average grain dimension) are essentially the same as those values determined for the TD-NiCr single crystals. It appears that the large grain TD-NiCr has approached the strength levels of TD-NiCr materials free of high angle grain boundaries under normal compression test strain rates (0.02/minute).

Tensile and Compression Thermal Activation Parameter Measurements

In order to evaluate the thermally activated deformation of TD-NiCr in tension and compression, the apparent activation enthalpy, ΔH, was determined using both conventional and differential testing methods. The expression chosen to calculate this value was that given by Conrad[27] and Evans and Rawlings[32]

$$\Delta H = -kT^2 \left(\frac{\partial \ln \dot{\varepsilon}}{\partial \sigma}\right)\left(\frac{\partial \sigma^*}{\partial T}\right) \qquad \ldots\ldots (13)$$

where k = Boltzman constant, T = absolute temperature, $\dot{\varepsilon}$ = strain rate, σ = applied stress, and σ^* = effective stress (component). The effective stress is related to the applied stress by the following relation

$$\sigma = \sigma_i + \sigma^* \qquad \ldots\ldots (14)$$

where σ_i = the athermal or internal stress (component). It is generally assumed that the internal stress is proportional to the

shear modulus of the material, whereby equation (13) can be modified to

$$\Delta H = -kT^2\left(\frac{\partial \ln \dot{\varepsilon}}{\partial \sigma}\right)\left[\left(\frac{\partial \sigma}{\partial T}\right) - \left(\frac{\sigma_i}{G}\frac{dG}{dT}\right)\right] \quad \ldots\ldots(15)$$

where G = shear modulus of the material.

As can be seen in Figure 10, the assumption that the internal stress is proportional to the shear modulus does not appear to be valid for TD-Nickel as studied by Petrovic[2,3] and for TD-NiCr materials examined in this study. The plot of values of σ_i/G versus temperature should be a straight line of zero slope if the above proportionality exists. However, using values of σi determined for TD-NiCr from relaxation tests and modulus data for Nichrome shown in Table III[28], a definite negative slope is observed. Consequently, Equations (12) and (14) were used to calculate activation enthalpies, thus eliminating any assumptions as to the nature of the internal stress.

The effective stress, σ^*, was determined as a function of temperature for all material states using stress relaxation tests and employing Equation (14). These data are shown in Figure 11. Values of $\partial\sigma^*/\partial T$ were determined from Figure 11.

Values of $\partial \ln \dot{\varepsilon}/\partial \sigma$ were obtained from differential strain rate change tests. Strain rate change transient behavior similar to that noted for TD-Nickel[2,3] was observed during the present study for TD-NiCr. This phenomenon, which was characterized by a greater stress sensitivity on low-to-high strain rate changes, was

observed in both tension and compression testing modes and in pure nickel as well as TD-Nickel and TD-NiCr. Because of the presence of these transient effects, measurements of $\partial \ln \dot{\varepsilon}/\partial \sigma$ were made during only high-to-low strain rate changes.

Using values of $\partial \sigma^*/\partial T$ and $\partial \ln \dot{\varepsilon}/\partial \sigma$ determined as indicated above and by Equation (13), the activation enthalpies, ΔH, for the polycrystalline and single crystal TD-NiCr were calculated. Figure 12 shows that, in the temperature range 816°C (1500°F) to 1260°C (2300°F), the activation enthalpy for all material conditions of TD-NiCr tested increased with increasing temperature. The fine grained TD-NiCr (Material D) had an extremely large increase in activation enthalpy to values of 16 ev. at 1260°C (2300°F). These data are similar to those determined for TD-Nickel [2,30] in a fine grained condition under similar testing conditions.

Figure 13 shows the grain size dependence of the activation enthalpy at 1093°C (2000°F) and 1260°C (2300°F). It is evident that the activation enthalpy decreases with increasing grain size. Also, for both Material D (see Figure 14) and the single crystal material, it was observed that the activation enthalpy decreased with increasing deformation.

In the thermal activation analysis of the deformation occurring in TD-NiCr at relatively high strain rates (0.02-0.2/minute) described in this section, it was necessary to perform both tensile and compression tests depending on the material condition and

availability. Since activation enthalpy data determined from tensile testing (Material D and L) and compression testing (Material B and single crystal) were compared directly, it was necessary to make the assumption that the deformation mechanisms were essentially the same for both testing modes. Despite the small amount of data available, concerning a direct comparison of tensile and compression data for face-centered cubic metals[31], it appeared that at the temperatures and strain rates used in the present study, this was a justified assumption.

Creep Testing

The primary quantitites of interest from the conventional creep testing of TD-NiCr materials performed in the present study were, 1) steady state creep rate, $\dot{\varepsilon}_s$, 2) creep strain as measured by the steady state creep strain, ε_s, and 3) the time to failure (rupture time), t_r. These were determined as a function of grain size for tensile creep at 1093°C (2000°F). Figure 15 shows typical creep curves (strain versus time) for material state B loaded to several fractions of its tensile yield stress determined at 1093°C (2000°F). The total creep curve is shown except for initial extension upon loading.

Classical three stage creep curves[31] were found for all TD-NiCr materials tested. The first stage (primary creep) region, which was characterized by a decreasing creep strain rate with increasing time, was followed by a region of constant strain rate

(steady state creep). The third stage (tertiary creep) preceding fracture had an increasing strain rate with time. However, for the polycrystalline TD-NiCr tested, tertiary creep strains were generally very low (below 0.005 inch/inch).

Figures 16 and 17 show the steady state creep rate as a function of applied stress for all materials tested. Figure 16 shows the steady state creep rate-stress dependence in the form of a power relationship

$$\dot{\varepsilon}_s \propto \sigma^n \qquad \ldots\ldots (16)$$

By plotting $\ln\dot{\varepsilon}_s$ versus $\ln\sigma$ where the stress exponent, n, can be determined as the slope of the curves. Figure 17 shows an exponential relationship of the form

$$\dot{\varepsilon}_s \propto \exp(\sigma) \qquad \ldots\ldots (17)$$

for the stress dependence of the steady state creep rate. By plotting $\ln\dot{\varepsilon}_s$ versus σ, the slope of the straight lines defines the stress sensitivity of the steady state creep rate, $\partial\ln\dot{\varepsilon}_s/\partial\sigma$. On the basis of the data available, it is not possible to distinguish which relationship better describes the creep data developed in this study.

According to Figure 16 the stress exponents for the steady state creep rate of the polycrystalline materials tested were between 6.0 and 7.3, with the slightly higher values applying to the behavior of the larger grain size TD-NiCr. Also shown in

this figure, are data recorded by Wilcox and Clauer[6] for creep of TD-NiCr of undetermined grain size at 1093°C (2000°F). A similar value of this stress exponent was given. However, it should be noted that these values are significantly lower than some published for TD-Nickel[2,6,8,9]. High stress exponents in TD-Nickel have usually been associated with high L/D ratios. The polycrystalline TD-NiCr studied in the present study had limited L/D ratios between 2-4.

Figures 16 and 17 indicate the extreme grain size sensitivity of the creep rate. The superior creep resistance of the large grain size material is evident.

The grain size dependence of the steady state creep rate is shown in Figure 18. Using interpolated and extrapolated values of steady state creep rate from Figure 17, $\ln\dot{\varepsilon}_s$ was plotted versus ln (average grain dimension) for the various TD-NiCr materials tested. Slopes of these plots for TD-NiCr ranged from 2 to 15.6. According to Raj and Ashby[19] (Equation 5), if diffusion controlled grain boundary sliding is the deformation mode, such a plot should yield a straight line with a slope of 2. It is evident that experimental values for TD-NiCr were somewhat higher. Similar relations have been observed for TD-Nickel[2,3] at 982°C (1800°F) and are also shown in Figure 18.

Ductility measurements of polycrystalline TD-NiCr during creep tests were limited to the primary and steady state creep regions. No clear grain size dependencies of the primary creep strain were

noted, but values did tend to increase with increasing stress for a constant grain size. Values were in the range of 1 to 3% elongation.

The stress-grain size dependence of the steady state creep strain is represented in Figure 19 for the materials tested. In general, the creep strain decreased with increasing grain size. The magnitude of this effect is evident in the fact that the large grained TD-NiCr (Material B) was more creep resistant at 9500 lb·in^{-2} (6.55 x 10^{7} N·M^{-2}) than the fine grained material (Material D) at 1500 lb·in^{-2} (1.03 x 10^{7} N·M^{-2}). However, the major effect on steady state creep strain was the extent to which steady state creep prevailed.

The rupture times for the various materials tested are shown in Figure 20 as related to applied stress. Again the superior creep properties of the large grain size TD-NiCr is evident. The applied stress resulting in a 100 hour creep life at 1093°C (2000°F) increased significantly from 1015 lb·in^{-2} (7 x 10^{6} N·M^{-2}) for Material D to 7100 lb·in^{-2} (4.9 x 10^{7} N·M^{-2}) for Material B.

The creep behavior of the single crystal TD-NiCr was also investigated. Figure 21 shows the conventional creep curves for TD-NiCr single crystal specimens oriented so that the loading axis was parallel to the <001> direction. It was noted that these curves were of the same general shape as those for the polycrystalline materials tested. Again, the three stage behavior is apparent. However, the major difference was the larger amount of tertiary

creep strain observed for the single crystals.

Figures 16 through 20 compare the creep data from the single crystal and polycrystalline TD-NiCr. It was observed that the single crystal material was more creep resistant (lower steady state creep rate and longer time to failure at a given stress level) than any of the polycrystalline materials. In compression at relatively high strain rates (see Figure 9), the large grain TD-NiCr and the single crystal had approximately the same yield stress. However, under creep loading, the single crystal TD-NiCr showed substantially better creep properties. The applied stress for a 100 hour creep life was found to be 12,500 $lb \cdot in^{-2}$ (8.62×10^7 $N \cdot M^{-2}$) for the single crystal TD-NiCr. The creep ductility of the single crystal was also greater than that observed for the polycrystalline TD-NiCr materials, except the very fine grain TD-NiCr.

More importantly, as shown in Figure 16, the stress exponent determined from the $\ln\dot{\varepsilon}_s$ versus $\ln\sigma$ curve for the single crystal TD-NiCr was significantly greater than the values determined for the polycrystalline TD-NiCr. The value of the stress exponent, n, determined for the single crystal TD-NiCr was 18.5 as compared to 6-8 for the polycrystalline materials. Whereas high stress exponents have been observed repeatedly for TD-Nickel[2,6,8,9], no such observations have been reported for polycrystalline TD-NiCr alloys in previous studies[6,7]. The present study indicates that the chracteristically high stress exponents are associated with

TD-NiCr when grain boundary effects have been minimized and dislocation motion prevails (i.e. single crystal).

Creep Thermal Activation Parameter Measurements

The calculation of the apparent activation enthalpy for creep may be performed using the following expression given by Conrad (27)

$$\Delta H = kT^2 \left(\frac{\partial \ln \dot{\varepsilon}}{\partial T}\right)_{\sigma^*} \qquad \ldots\ldots (18)$$

where $\dot{\varepsilon}$ = the creep rate, T = absolute temperature and σ^* = the effective stress given by Equation (14). Incorporating the assumption that the internal stress, σ_i, is proportional to the shear modulus, G, Equation (18) can be expressed in the form

$$\Delta H = kT^2 \left(\left(\frac{\partial \ln \dot{\varepsilon}}{\partial T}\right)_{\sigma} + \left(\frac{\partial \ln \dot{\varepsilon}}{\partial \sigma}\right)_T \left(\frac{\sigma_i dG}{G\ dT}\right)\right) \qquad \ldots\ldots (19)$$

Creep activation enthalpies for TD-NiCr in the present study were calculated using Equation (19). Values for $(\partial \ln \dot{\varepsilon}/\partial T)$ were determined from differential temperature creep tests; whereas Figure 17 was used for $(\partial \ln \dot{\varepsilon}/\partial \sigma)$. Values for (dG/dT) were taken from Table III.

Two major assumptions were made by using Equation (19). Since no internal stress measurements were made under creep conditions, the internal stress was approximated by the applied stress (i.e. $\sigma_i = \sigma$). Also, even though the internal stress was found not to be proportional to the shear modulus in tension and compression

(Figure 10), this assumption was still implicit in Equation (19). Therefore, the term $(\sigma_i/G)(\partial G/\partial T)$ must be considered only a first approximation for the true internal stress correction. Similar methods have been used previously in the thermal activation analysis of the creep deformation of TD-Nickel[2,3].

Figures 22 through 24 represent the creep activation enthalpies, ΔH, for the TD-NiCr materials investigated in the present study. The activation enthalpies are shown as a function of stress and strain. All measurements were made during steady state creep.

Figure 22 shows the activation enthalpy values for the TD-NiCr polycrystalline materials (Materials B, L, D), along with those determined for the single crystal TD-NiCr. These data are plotted as a function of applied stress. For reference, the activation enthalpy band for self-diffusion in nickel and nichrome (approximately 20% chromium) as found in the literature[6,7] is also indicated.

It was determined that for the fine grained TD-NiCr (Materials D and L), creep activation enthalpies were very near the self-diffusion values (~3ev). As seen in Figure 22, the activation enthalpies of these material states were not noticeably stress dependent.

The behavior of the large grained Material B was somewhat different. Activation enthalpies for this material state were in the range 4 to 4.5 eV which is higher than the enthalpy of self-diffusion in nichrome and also higher than the activation enthalpy

for creep in the fine grained TD-NiCr. This is shown particularly well by comparing the enthalpies determined for Material L and Material B at a constant stress (~6500 $lb \cdot in^{-2}$(4.48×10^7 $N \cdot M^{-2}$)). The value determined for Material B is approximately 1.5 eV higher than that for Material L. It was also observed that the activation enthalpies for Material B in creep were somewhat stress dependent with the enthalpy decreasing with increasing stress over the range of stresses examined. It was not possible to determine the strain dependence of the activation enthalpy for Material B because of the extremely low creep ductilities observed for this material condition.

The creep activation enthalpies for the single crystal material were determined and are also represented as a function of stress in Figure 22. Single crystal activation enthalpies were in the range 4 to 4.5 eV. Indicating that the higher values were characteristic of the deformation mode present in the single crystal material (i.e. dislocation motion). Activation enthalpies were moderately stress dependent with decreasing values at higher stresses. Figure 24 shows the strain dependence of the activation enthalpy for the single crystal TD-NiCr at two different applied stress levels. While low values (~3 eV) were generally observed near the start of steady state creep, the activation enthalpy increased to values near 4.5 ev with increasing creep strain.

Fractography of TD-NiCr Materials

The fracture regions of elevated temperature tensile specimens

were examined using light-optical microscopy and scanning electron microscopy. Material D and the single crystal TD-NiCr were chosen for this investigation because they represented the largest degree of difference in mechanical behavior and fracture mode. Results were compared to fractured specimens of Material D deformed at room temperature (25°C (77°F)).

Figures 25 and 26 show the characteristics of room temperature and elevated temperature deformation. Material D, as shown in Figure 25, was observed to be ductile at room temperature. Localized necking was exhibited around the fracture region after approximately 20% plastic deformation. The appearance of the fracture surface under the scanning electron microscope showed typical features of ductile failures, i.e. dimpled and cusped regions. The size of these features was generally much less than the average grain dimension indicating an intragranular deformation mode. The particles observed on the fracture surface of the room temperature specimen (see Figure 25a) were of too large a size to be thoria particles but did appear to match the size of inclusions (probably chromium oxide) observed in unetched micrographs of the various TD-NiCr materials examined.

Figure 26 shows the appearance of this material condition after elevated temperature tensile deformation. It can be seen that even though 11% plastic deformation had occurred, no necking of the specimen was noted. The scanning electron microscope micrograph shows features resembling the grain structure of this material.

The size of these nodular features is comparable to the average grain dimension, 0.0037mm. Intergranular (grain boundary) fracture was indicated. Further evidence for this failure mode is suggested by Figure 27 which shows a micrograph of the region where failure occurred. The presence of grain boundary separation and cavitation is evident.

The behavior of Material D was typical of all the polycrystalline TD-NiCr materials tested. All appeared to have grain boundary separations and cavitations near the fracture surface. However, the extent of the cavitation did decrease with increasing grain size for tensile deformation indicating a possible decrease in the contribution of the grain boundary mechanisms with increasing grain size. Tensile creep specimens of the polycrystalline materials tested also were observed to have similar fracture characteristics. However, no fracture surfaces of creep specimens could be observed directly using scanning electron microscopy because these surfaces were badly damaged by oxidation after fracture.

The single crystal TD-NiCr creep specimen is shown in Figure 28 following testing at 1093°C (2000°F). The surfaces of the gage section which were metallographically polished prior to testing formed a coherent, stable oxide layer in the testing atmosphere. However, the most significant observation was the extent of plastic flow during the creep test. A region of necking was found adjacent to the fracture surface which was extensive at the high creep stresses. This behavior was extremely different than that observed

for the polycrystalline TD-NiCr materials tested in creep and tension at elevated temperatures. The polycrystalline TD-NiCr failed in a very brittle manner with no necking but by the formation of intergranular cavitation, whereas the single crystal material, having no high angle grain boundaries, promoted deformation by dislocation motion. The absence of grain boundaries in the single crystal also promoted high ductilities and increased failure times by greatly reducing damaging effects of void formation and cavitation. Evidence of the dislocation motion was noted in the observation of slip lines on the polished (but oxidized) surfaces of the creep specimen after fracture. As shown in Figure 28, these features appeared as straight segmented features perpendicular to the stress axis. The slip lines were well developed as opposed to those shown after 3% plastic strain in tension (see Figure 5). This is characteristic of the higher degree of plastic deformation in the creep specimen.

CHAPTER VI

DISCUSSION

It has been observed for TD-Nickel that, with increasing L/D ratio and increasing grain size, major changes in elevated temperature creep behavior occur. Specifically, stress exponents and creep activation enthalpies have been shown to be very sensitive to these variables. For relatively small, equiaxed grain structures[8,33], stress exponents were reported to be in the range 6-7 and activation enthalpies were near the self-diffusion enthalpy (3 ev). With increasing L/D ratio[2,3,9], stress exponents were also shown to increase to values as high as 40 with activation enthalpies of 8-10 ev.

Recently, it has been proposed[3,21] that such behavior can be explained in terms of the relative contribution of grain boundary sliding and dislocation deformation modes as shown in Equation (6). In creep, it is suggested that with increasing L/D ratio and increasing grain size, the nature of the deformation mode changes from diffusion controlled grain boundary sliding to dislocation motion. Therefore, the resultant high stress exponents and activation enthalpies are thought to be characteristic of the dislocation motion mode. However, prior to the present study, the nature of this deformation mode could not be examined because of the complicating factor of the presence of high angle grain boundaries in these materials.

It has been indicated above that previous studies concerning the elevated temperature deformation of TD-NiCr have not reported the strong grain size or shape sensitivity of the creep activation enthalpy and stress exponent that was shown to be characteristic of TD-Nickel. However, these investigations have been limited to generally small grain sizes and relatively equiaxed grain shapes, and have not directly dealt with the effect of these parameters on the elevated temperature deformation mechanisms.

Characterization of the Dislocation Deformation Mode in TD-NiCr

In the present study it has been directly observed that relatively high activation enthalpies for elevated temperature deformation and high stress exponents are reflective of the dislocation deformation mode in TD-NiCr. Using single crystal creep specimens, stress exponents of 18.5 and creep activation enthalpies as high as 4.5 ev were found. Since this material contained no high angle grain boundaries, the contribution of grain boundary deformation mechanisms to the overall elevated temperature mechanical behavior was effectively zero. Therefore, according to Equation (6), the single crystal data were totally representative of the dislocation deformation mechanism present in TD-NiCr.

The elevated temperature mechanical testing of the single crystal TD-NiCr indicated that deformation by this dislocation mechanism was also significantly more difficult than by alternate processes (diffusion controlled grain boundary sliding being con-

sidered the only significant alternate process). This was manifest in the high yield stress and superior creep resistance of the single crystal material in comparison to that observed for the polycrystalline TD-NiCr.

The findings of the present study also indicate that the nature of the dislocation deformation mechanism present in TD-NiCr at elevated temperatures may be similar to that proposed for dislocation motion in TD-Nickel by Petrovic[3,21]. As shown previously, it was proposed that both dislocation glide and climb in dispersion strengthened materials as TD-Nickel are significantly influenced by stresses in the matrix at thoria particles which arise from surface tension effects at the particle-matrix interface. These stresses are as shown in Equation 7a and 7b. It was indicated that significant interactions could occur between these stress fields and those of the matrix dislocations, thus exerting "pinning" forces on the dislocations near the particles. Most importantly, these effects will occur at elevated temperatures since not even vacancy diffusion can relieve the surface tension stresses. Because of the basic similarities of the thoria dispersion and the matrix phase in TD-Nickel and TD-NiCr, it seems likely that such effects should also be present in TD-NiCr.

Using this analysis to evaluate the single crystal TD-NiCr, it is possible to consider the dislocation-particle interaction as the source of the high activation enthalpies observed. The interaction energy, U, for this situation was shown by Petrovic[3,21]

to be of the form

$$U = 2R_o E_s b \qquad \ldots\ldots (20)$$

where R_o = particle radius, E_s = surface energy, and b = Burgers vector. Substituting corresponding values of $R_o = 100\text{Å}$, $E_s = 680$ ergs/cm^2 (34)* and $b = 2.50\text{Å}$ (38), the calculated value for the particle-matrix interaction energy in TD-NiCr is 21.2 ev. This is significantly higher than the self-diffusion enthalpy (~3 ev). Also, the shear stress to effectively remove the dislocation from the vicinity of the thoria particle, τ, can also be estimated by considering the maximum interaction as

$$E_s b = \tau b R_o \; ; \quad \tau = \frac{E_s}{R_o} \qquad \ldots\ldots (21)$$

thereby yielding a value of 9.86×10^3 lb·in^{-2} (6.80×10^7 N·M^{-2}). This shear stress is in the order of the stress required to operate a Frank-Read source (i.e. Gb/d, where d = the distance between pinning points). These calculations indicate that the surface tension effects around the thoria particles may be a significant factor in the elevated temperature deformation of TD-NiCr.

These calculations are also important in relation to the observed yield strength for the single crystal TD-NiCr. At 1093°C (2000°F) the critical resolved shear stress was found to be in approximately 6.3×10^3 lb·in^{-2} (4.31×10^7 N·M^{-2}) depending only

---

*E_s determined for nichrome (Ni-20Cr) at 1060°C (1940°F).

slightly on orientation. The experimental values do show good correlation with theoretical values when considering the approximate nature of the theoretical calculations, and that they were based on the maximum dislocation-particle interaction.

Calculations performed in the present study appear to give higher theoretical stresses and activation enthalpies associated with the dislocation-particle interaction of TD-NiCr than those found in the work of Petrovic[3,21] for TD-Nickel. However, this is a false indication arising from the different data sources being used. Petrovic's calculations were made using the surface energy of TD-Nickel as being equal to the corresponding value for pure nickel[39] (E_s = 620 ergs/cm^2). More recent data by Murr[40] determined for both pure nickel and TD-Nickel indicates that the surface energies of these materials may be somewhat greater than those used in the previous calculations. Surface energy values of 860 ergs/cm^2 for pure nickel and 1080 ergs/cm^2 for TD-Nickel were reported.

In comparing the surface energies of pure nickel (860 ergs/cm^2) and nichrome (680 ergs/cm^2), it would appear that the particle-dislocation interaction of the type being considered would be greater in TD-Nickel than in TD-NiCr. The relative magnitude of these interactions should be in direct proportion to their surface energies of the respective matrix materials (i.e. E_s^{NiCr}/E_s^{Ni}). On the basis of these considerations, the effective particle-dislocation interaction in TD-NiCr should be approximately 0.63 to 0.77

the magnitude of that found in TD-Nickel. Consequently, it is expected that the measured activation enthalpies for dislocation motion in TD-NiCr may be significantly lower than values determined for TD-Nickel, but are still expected to be greater than self-diffusion enthalpies.

Two other characteristics observed only during the elevated temperature deformation of the single crystal TD-NiCr were the particularly high internal stress values measured in compression tests (shown in Figure 29) and the high stress exponent of the steady state creep rate. Both of these observations are predicted by the dislocation-particle interaction being considered.

Because of the extremely high interaction energy, U, it is logical to assume that the thoria particle constitutes an athermal dislocation barrier (a barrier which cannot be overcome by usual thermal activation). For thermal activation to occur, a portion of the effective stress, σ^*, is required to lower the interaction energy into the range of thermal activation, thus acting in a similar way, and in addition to, the internal stress as described by Conrad[27]. This effectively increases the internal stress, and since U is very large, the internal stress may be a large fraction of the applied stress. For TD-NiCr in single crystal form the internal stress was in the order of 0.8-0.9 of the applied stress.

The high stress exponent of the steady state creep rate ($\partial \ln \dot{\varepsilon}/\partial \sigma$) of the single crystal material can be rationalized in

terms of Equation (8) where ΔH is given by

$$\Delta H = U - \sigma^* bA \qquad \ldots\ldots(22)$$

Here, σ^* = the experimentally determined effective stress and A = activation area. It can be seen that the strain rate is exponentially related to the effective stress. Upon differentiation, the stress exponent, n, becomes

$$n = \frac{\partial \ln \dot{\epsilon}}{\partial \ln \sigma} = \sigma^* bA/kT \qquad \ldots\ldots(23)$$

Assuming values of $\sigma^* = 0.1\text{-}0.2\sigma$, and $A = 2 \times 10^{-12} cm^2$ (3), stress exponents much larger than those commonly observed for pure metals may arise.

Estimation of the Relative Contributions of Grain Boundary Sliding and Dislocation Motion

By considering diffusion controlled grain boundary sliding and dislocation motion to be parallel-concurrent processes, it was possible to examine the relative contributions of these mechanisms in the elevated temperature deformation of TD-NiCr. The terminology of parallel-concurrent is taken to mean the simultaneous and independent operation of both processes being considered. Only under these conditions can the overall creep strain rate, $\dot{\epsilon}_s$, be represented as the sum of the strain rate due to grain boundary sliding, $\dot{\epsilon}_{GBS}$, and the strain rate due to dislocation motion, $\dot{\epsilon}_{DIS}$ (35),

$$\dot{\varepsilon}_s = \dot{\varepsilon}_{GBS} + \dot{\varepsilon}_{DIS} \qquad \ldots\ldots(24a)$$

$$1 = \dot{\varepsilon}_{GBS}/\dot{\varepsilon}_s + \dot{\varepsilon}_{DIS}/\dot{\varepsilon}_s \qquad \ldots\ldots(24b)$$

(Equation (24a) is the uniaxial strain rate equivalent of Equation (6).)

In the present study, the dislocation contribution to the elevated temperature deformation process of TD-NiCr was assumed to be that observed for the single crystal material. In the previous section it was shown that this behavior could be represented in the form of Equation (8) and could be altered for Equation (24) using $\dot{\gamma} = \sqrt{2}\dot{\varepsilon}$ and $\tau = \sigma/2$ for polycrystalline materials. Similarly, the contribution of grain boundary sliding was considered to be that developed by Raj and Ashby[19] given in Equation (5).

Using the data from Figures 16 and 17, along with extrapolations of these values, an estimation of the relative dislocation motion contribution was made in terms of $\dot{\varepsilon}_{DIS}/\dot{\varepsilon}_s$ for the various material conditions of TD-NiCr as a function of applied stress. Values of $\dot{\varepsilon}_{DIS}$ and $\dot{\varepsilon}_s$ were respectively given by the single crystal and polycrystalline creep rates corresponding to the applied stress values.

It was determined that in creep, the deformation behavior of the fine grained TD-NiCr (Materials D and L) was predominantly governed by the diffusion controlled grain boundary sliding deformation mode ($\dot{\varepsilon}_{DIS}/\dot{\varepsilon}_s \sim 0$). Only in the large grain size TD-NiCr

(Material B) did dislocation motion occur to a significant extent. Furthermore, as shown in Figure 30, the dislocation motion deformation mode in Material B prevailed only at relatively high values of the applied creep stress. These observations are the direct consequence of the high stress necessary to operate this mechanism, as indicated previously, and the extreme stress dependence of the steady state creep rate associated with dislocation motion in TD-NiCr.

In view of the difficult nature of the dislocation motion, the material will seek an easier deformation mode. In the present analysis, the alternate mode is diffusion controlled grain boundary sliding. At the low stresses and high temperatures involved in creep testing, it has been observed that this deformation mode does predominate in the polycrystalline TD-NiCr materials. Because of their small grain size and L/D ratios, it is evident from Equation (5) that a relatively large grain boundary sliding contribution is to be expected. Also, as proposed in Equation (8), the stress dependence of the strain rate resulting from dislocation motion is exponential through Equation (22). Consequently, a larger stress dependence is predicted for dislocation motion than for grain boundary sliding. This, therefore, promotes the increase in the relative contribution of dislocation motion (decrease in grain boundary sliding) with increasing stress.

Further support for the estimation of the relative contributions of dislocation motion and grain boundary sliding in TD-NiCr

proposed in the present study is also given in Figure 16. The point where Material B and the single crystal material would exhibit identical steady state creep rates for a given applied stress was extrapolated to be 20.8×10^3 lb·in^{-2} (14.3×10^7 N·M^{-2}). The creep rate associated with this stress value was 0.0140/min. In elevated temperature compression tests at 1093°C (2000°F), Material B and single crystal material of an <110> orientation were found to have nearly identical yield strengths. The strain rate of these tests was approximately 0.02/minute.

The literature contains no mention of previous attempts to estimate the relative contributions of grain boundary sliding and dislocation motion in dispersion strengthened materials as TD-Nickel and TD-NiCr. Limited work has been reported on aluminum-copper alloys containing a dispersion of $CuAl_2$ particles[36]. Using techniques with which to measure the strain resulting from grain boundary sliding directly, it was determined that surprisingly high grain boundary sliding contributions existed in these alloys when compared to alloys of similar composition but of a single phase nature. In the present study, methods of determining grain boundary strains[37] were attempted. However, the extremely small total strains observed in TD-NiCr made the results of these methods inconclusive.

Effects of Deformation Mode on Material Performance

The influence of the deformation mode in dictating material

performance was also examined. It was shown that the observed trends in the 1) yield stress, 2) internal stress, 3) stress sensitivity of the creep rate, and 4) activation enthalpy of TD-NiCr could be rationalized on the basis of these considerations.

It has been proposed that the creep behavior of the polycrystalline TD-NiCr containing fine, equiaxed grains (Materials D and L) is predominantly controlled by diffusion controlled grain boundary sliding. Figure 16 also indicates that the deformation behavior of these material conditions of TD-NiCr under normal tensile testing strain rates (0.02/minute) may also be governed by the same process, but with dislocations becoming increasingly important. Tensile test results on TD-NiCr in the present study (Figure 4) and those previously reported[4,23] indicate that the elevated temperature yield stress of these materials is very sensitive to average grain dimension in the small grain size region (below 0.020mm, average grain dimension) for relatively equiaxed grain structures. Such a grain size sensitivity is predicted when grain boundary sliding is the dominant deformation mode as shown in Figure 5.

It was also observed that for larger grain size (0.020-0.19mm, average grain dimension), the yield stress did not show a similarly strong grain size sensitivity. This seems reasonable in view of the fact that, with increasing grain size, the relative contribution of dislocation motion to the overall deformation process likewise increases. The present dislocation models of elevated temperature

deformation do not predict a strong grain size dependence.

Internal stress measurements made in tension and compression indicate that there is a definite transition in the elevated temperature deformation behavior occurring with grain size in TD-NiCr. Figure 29 shows that while generally high values of internal stress are associated with the large grain size and single crystal materials, lower values have been found to exist for the small, equiaxed grain structures. As shown in a previous section, high internal stresses are characteristic of dislocation motion as a result of the athermal nature of the barrier imposed to dislocations at thoria particles. However, it has been indicated by Ashby[20] that the internal stress, σ_i, in dispersion strengthened materials, when grain boundary sliding is the predominant process, may be proportional to the shear modulus, G, and of the form

$$\sigma_i \propto \frac{G}{d} \qquad \ldots\ldots(25)$$

where d = the interparticle spacing. Such effects may give higher internal stresses than observed in pure materials but are not expected to give abnormally high values as predicted by dislocation motion.

The stress sensitivities of the steady state creep rate, as given by $\partial \ln \dot{\varepsilon}_s / \partial \ln \sigma$ in Figure 16, were relatively low for all polycrystalline TD-NiCr materials tested (n = 6-7.3). Only a slight increase in stress exponent was noted with increasing grain size up to an average grain dimension of 0.19mm. This also indicates

the predominance of grain boundary sliding under normal creep loading conditions, with dislocation motion only becoming significant at relatively high values of the applied stress. According to Equation (5) for grain boundary sliding, the stress exponent should be of a value 1. However, Ashby[20] suggests that larger values can arise from the presence of internal stresses as indicated by Equation (25).

As indicated by the observed behavior of the TD-NiCr single crystal material in creep, high stress exponents of the strain rate are characteristic of dislocation motion. Observed values were significantly higher than those noted when grain boundary sliding was present.

Activation enthalpies determined in creep support the conclusion that grain boundary sliding was the major deformation mode in the small, equiaxed grain structures of TD-NiCr during creep testing. Values of the creep activation enthalpy for these materials were near the self-diffusion value (~3 ev) and independent of stress and strain. With increasing contribution of dislocation motion, the observed creep activation enthalpies increased to values greater than 3 ev. As shown previously, the high activation enthalpies and their stress and strain dependence can be predicted by considering the thoria particle-dispersion interaction of the type proposed by Petrovic[3,21].

Despite the above, it was noted that activation enthalpies determined in creep for single crystal TD-NiCr were generally less

than those values determined in TD-Nickel where dislocation motion was predicted to predominate (i.e. large L/D ratios). An explanation for this observation can be found in the essence of the particle-dislocation interaction. The magnitude of the interaction is directly related to the surface energy of the matrix material. From the literature it was found that the surface energy of nichrome was approximately 0.63 to 0.77 that of pure nickel and TD-Nickel. Consequently, from these basic considerations,it was expected that observed activation energy values associated with dislocation motion in TD-NiCr would be relatively low but still above the self-diffusion enthalpy.

For testing at normal tension and compression test strain rates, it is suggested that high activation enthalpies can be observed even when grain boundary sliding is the predicted deformation mode. By the nature of the differential strain rate test, the strain rate is changed discontinuously by as much as a factor of ten (0.02-0.2/minute). It is possible that such rapid changes in strain rate can effectively change the deformation mode or their relative contributions. Therefore, the observed decrease in activation enthalpy with increasing grain size found in tensile and compression tests of TD-NiCr at elevated temperatures (see Figure 13), may be apparent. Similar behavior has been reported for activation enthalpies in TD-Nickel determined from tensile tests[2,3]. Under such conditions, it is possible that the decrease in activation enthalpy with increasing grain size is a direct result

of the stress dependence of the activation enthalpy.

Elevated Temperature Deformation of Dispersion Strengthed Materials

The present study indicates that elevated temperature deformation in TD-NiCr, when dislocation motion is the dominant deformation mechanism, is significantly more difficult than when alternate processes (i.e. diffusion controlled grain boundary sliding) are present. Consequently, the maximum strength and creep resistance of TD-NiCr will be related to the single crystal form of this material. In this material condition, the elevated temperature deformation will be dictated entirely by dislocation motion.

It has been shown that the relatively high activation enthalpies and stress exponents commonly observed in dispersion strengthened materials are the direct result of the dislocation deformation mode. The results of the present study also indicate that the theoretical analysis proposed by Petrovic[3,21] can describe the behavior characteristics of this deformation mode.

The relative contributions of dislocation motion and grain boundary sliding to the overall deformation process in TD-NiCr is strongly dependent on grain size, stress and strain rate. The grain boundary sliding mode will tend to predominate under creep conditions (i.e. low stress and high temperature) unless the grain size is significantly large and/or the applied stresses are made relatively high.

It would seem that the results of the present study are characteristic of all dispersion strengthened materials which are of a similar nature as TD-NiCr. Such materials include the TD-Nickel base alloys and to a certain extent the sintered aluminum powder (SAP) alloys. All of these materials have been shown to exhibit similarly high values of activation enthalpy and stress exponent depending on material and testing related variables. The results of the present study may also be applied to elevated temperature deformation of certain tungsten alloys[41] containing dispersions of stable, sub-micron size voids. High stress exponents have been observed for the creep of such alloys.

While the characteristics and basic implications of the present study may apply to these dispersion strengthened systems, the relative contributions of dislocation motion and grain boundary sliding will be strongly dependent on the nature of the materials under consideration. From the analysis presented, it is expected that grain size and shape will be extremely important parameters in determining the relative contributions of dislocation motion and grain boundary sliding.

It is also proposed, on the basis of theoretical considerations[3,21], that the maximum strength attainable in the dispersion strengthened material (given by dislocation motion) will increase with increasing volume fraction of dispersed phase material and surface energy of the matrix material and with decreasing dispersed particle radius.

CHAPTER VII

CONCLUSIONS

The following conclusions seem warranted on the results and discussion of the present investigation concerning the elevated temperature deformation of TD-Nickel Chromium (TD-NiCr):

1. The elevated temperature yield strength of TD-NiCr increased with increasing grain size reaching a maximum value for the single crystal material.

2. The crystallographic nature of the slip process in the single crystal TD-NiCr was the same as that present in classical non-thoriated face-centered-cubic metals. The characteristics of this process (i.e. yield stress and strain hardening behavior) were strongly temperature dependent in the range 25°C (77°F) to 1260°C (2300°F).

3. It was shown that in TD-NiCr measurements of internal stress made in tension and compression were not proportional to the shear modulus. Consequently, to calculate real activation enthalpies in tension and compression, necessary corrections must be made for the observed internal stresses.

4. In creep, the activation enthalpy was observed to be near the self-diffusion enthalpy for the small, equiaxed grain structures. The activation enthalpy increased with increasing grain size, reaching maximum values for the single crystal material.

5. The stress exponent of the steady state creep rate was

found to increase only slightly with grain size for the polycrystalline TD-NiCr. The maximum stress exponent was observed for the single crystal material which was significantly higher than polycrystalline values.

6. The characteristics of the dislocation motion deformation mode present in TD-NiCr (as observed in the single crystal material) are those of high creep activation enthalpies (relative to the self-diffusion enthalpy) and high stress exponents. The activation enthalpy for this deformation mode is both strain and stress dependent.

7. The present study suggests that the nature of the dislocation motion in TD-NiCr may be governed by surface tension stresses present in the matrix around thoria particles. The theoretical considerations of this mechanism successfully predict the characteristics observed for TD-NiCr and their relative magnitude with respect to TD-Nickel.

8. The overall elevated temperature deformation behavior of TD-NiCr can be understood on the basis of the concurrent-parallel operation of dislocation motion and diffusion controlled grain boundary sliding. The nature of the behavior observed will be determined by the relative contribution of these processes, which in turn, is controlled by the material and test related variables (i.e. grain size and shape, temperature, stress and strain rate).

REFERENCES

1. G. S. Doble, Ph.D. Thesis, Case Western Reserve University, November, 1967.

2. J. J. Petrovic and L. J. Ebert, Met. Trans., 1973, Vol. 4, pp. 1301-1308.

3. J. J. Petrovic, Ph.D. Thesis, Case Western Reserve University, July, 1972.

4. R. D. Kane, M. S. Thesis, Case Western Reserve University, January, 1973.

5. D. Webster, Trans. ASM, 1969, Vol. 62, pp. 936-947.

6. B. A. Wilcox and A. H. Clauer, Acta Met., 1972, Vol. 20, pp. 743-757.

7. B. A. Wilcox and A. H. Clauer, Met. Sci. J., 1969, Vol. 3, p. 26.

8. B. A. Wilcox and A. H. Clauer, Met. Sci. J., 1967, Vol. 1, p. 86.

9. B. A. Wilcox and A. H. Clauer, Trans. AIME, 1966, Vol. 236, p. 570.

10. A. Akhtar and E. Teghtsoonian, Met. Trans., 1971, Vol. 2, p. 2762.

11. J. D. Whittenberger, Met. Trans., 1973, Vol. 4, p. 1475.

12. G. S. Ansell and J. Weertmen, Trans. AIME, 1959, Vol. 215, p. 838.

13. B. A. Wilcox and A. H. Clauer, in Oxide Dispersion Strengthening, Vol. 47, Gordon and Breach, New York, 1968, p. 323.

14. P. Guyot, in Oxide Dispersion Strengthening, Vol. 47, Gordon and Breach, New York, 1968, p. 405.

15. J. Friedel, Dislocations, Pergamon Press, New York, 1964, p. 373.

16. R. Lagneborg, J. Mat. Sci., 1968, Vol. 3, p. 596.

17. J. Tien, B. Kear and G. Leverant, Scripta Met., 1972, Vol. 6, p. 135.

REFERENCES (Continued)

18. R. W. Fraser and D. J. I. Evens, in Oxide Dispersion Strengthening, Vol. 47, Gordon and Breach, New York, 1968, p. 375.

19. R. Raj and M. F. Ashby, Met. Trans., 1971, Vol. 2, p. 1113.

20. M. F. Ashby, Scripta Met., 1969, Vol. 3, p. 837.

21. J. J. Petrovic and L. J. Ebert, Met. Trans., Vol. 4, 1973, pp. 1309-1314.

22. R. E. Allen, in Superalloys - Processing, Proceedings of the 2nd International Conference, Met. Soc. AIME, Metals and Ceramics Information Center, 1972, Section X.

23. R. D. Kane and L. J. Ebert, NASA Contract NGR 36-003-094, Annual Status Report, July, 1973.

24. R. T. DeHoff and F. N. Rhines, Quantitative Microscopy, McGraw-Hill, New York, 1968, p. 201.

25. R. L. Fullman, R. P. Carrekar, Jr., and J. C. Fisher, Trans. AIME, 1953, Vol. 197, p. 657.

26. J. Weertman and J. R. Weertman, in Physical Metallurgy, ed. R. W. Cahn, North-Holland, 1970, p. 924.

27. H. Conrad, Mechanical Behavior of Materials at Elevated Temperatures, McGraw-Hill, New York, 1961, p. 149.

28. T. YaBenieva and I. G. Polotsky, Physics of Metals and Metallography, April, 1961, p. 111.

29. D. K. Bowens and J. W. Christian, Phil. Mag., 1966, Vol. 12, p. 369.

30. A. Lasalmonie and M. Sindzinger, Acta Met., 1971, Vol. 19, p. 57.

31. G. E. Dieter, Mechanical Metallurgy, McGraw-Hill, 1961, p. 340.

32. A. G. Evans and R. D. Rawlings, Phys. Stat. Sol., 1969, Vol. 84, p. 9.

33. B. A. Wilcox and A. H. Clauer and W. B. Hutchinson, NASA Contract NAS 3-11167, Final Report, March 1971.

34. L. E. Murr, R. J. Horylev and G. I. Wong, Surface Science, 1971, Vol. 26, p. 184.

REFERENCES (Continued)

35. R. C. Gifkins, J. of Mat. Sci., 1970, Vol. 5, p. 156.

36. Y. Ishida, A. W. Mullendore, and N. J. Grant, Trans. AIME, 1964, Vol. 230, p. 1454.

37. R. N. Stevens, Met. Reviews, 1966, Vol. 11, p. 129.

38. D. H. Kilpatrick and J. D. Young, Met. Trans., 1970, Vol. 1, p. 955.

39. P. G. Shewmon, in Recrystallization, Grain Growth and Textures, ed. ASM, Metals Park, 1966, p. 173.

40. L. E. Murr, P. J. Smith and C. M. Gilmore, Phil. Mag., 1968, Vol. 17, p. 89.

41. P. K. Wright III, Private Communication.

TABLE I

CHEMICAL COMPOSITION OF TD-NiCr SHEET

LOT 3829

Element	Weight %
C	0.0174
S	0.006
Cr	19.0
ThO_2	2.11
Ni	Balance

TABLE II

MATERIAL CONDITIONS OF TD-NiCr*

Material Designation	Reductions in Thickness by Transverse Cold Rolling	Average Grain Dimension
B	0%	0.190 ± 0.014mm
L	22%	0.0086 ± 0.0026mm
D	48%	0.0037 ± 0.00035mm

L/D Ratio Between 2-4 for
All Materials

*For all materials, the starting material (prior to cold rolling) was the as-received 0.1 inch thick TD-NiCr sheet annealed at 1316°C (2400°F) for 1 hour in argon. Final grain size was established by an identical annealing treatment after cold rolling.

TABLE III

SHEAR MODULUS DATA FOR PURE NICHROME (Ni-20 Cr)*

Temperature °F	Temperature °C	Shear Modulus (G) lb/in^2	dG/dT $lb/in^2 \cdot °C$
77	25	11.76×10^6**	--
1100	593	9.87×10^6	-4.77×10^3
1500	816	8.65×10^6	-6.48×10^3
1800	982	7.40×10^6	-8.10×10^3
2000	1093	6.42×10^6	-8.73×10^3
2300	1260	4.87×10^6**	-9.46×10^3

*Data from Reference 28 Using $E/(2)(1 + \nu)$ where

ν = Poisson's Ratio $\simeq$ 0.33.

**Extrapolation of Given Data.

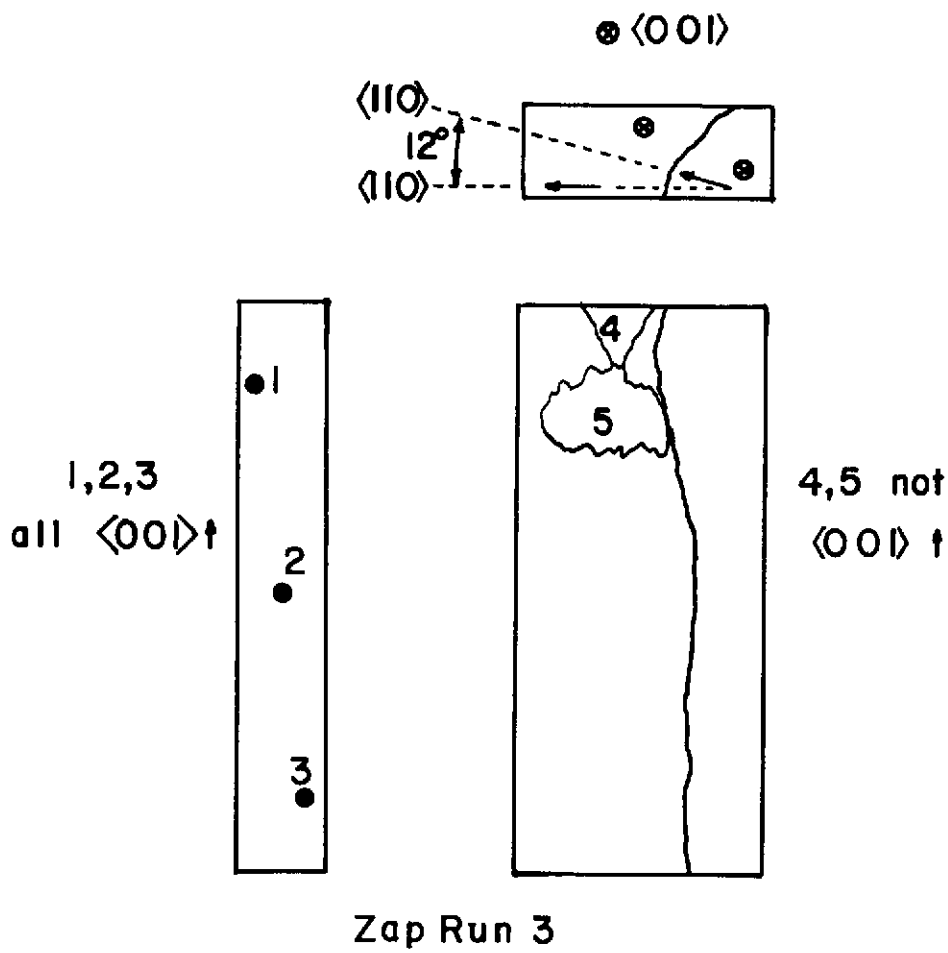

Figure 1 - TD-NiCr Bi-crystal supplied by Dr. R.E. Allen (Powder Metallurgical Alloys, General Electric Company). Note 12° rotation of major grains.

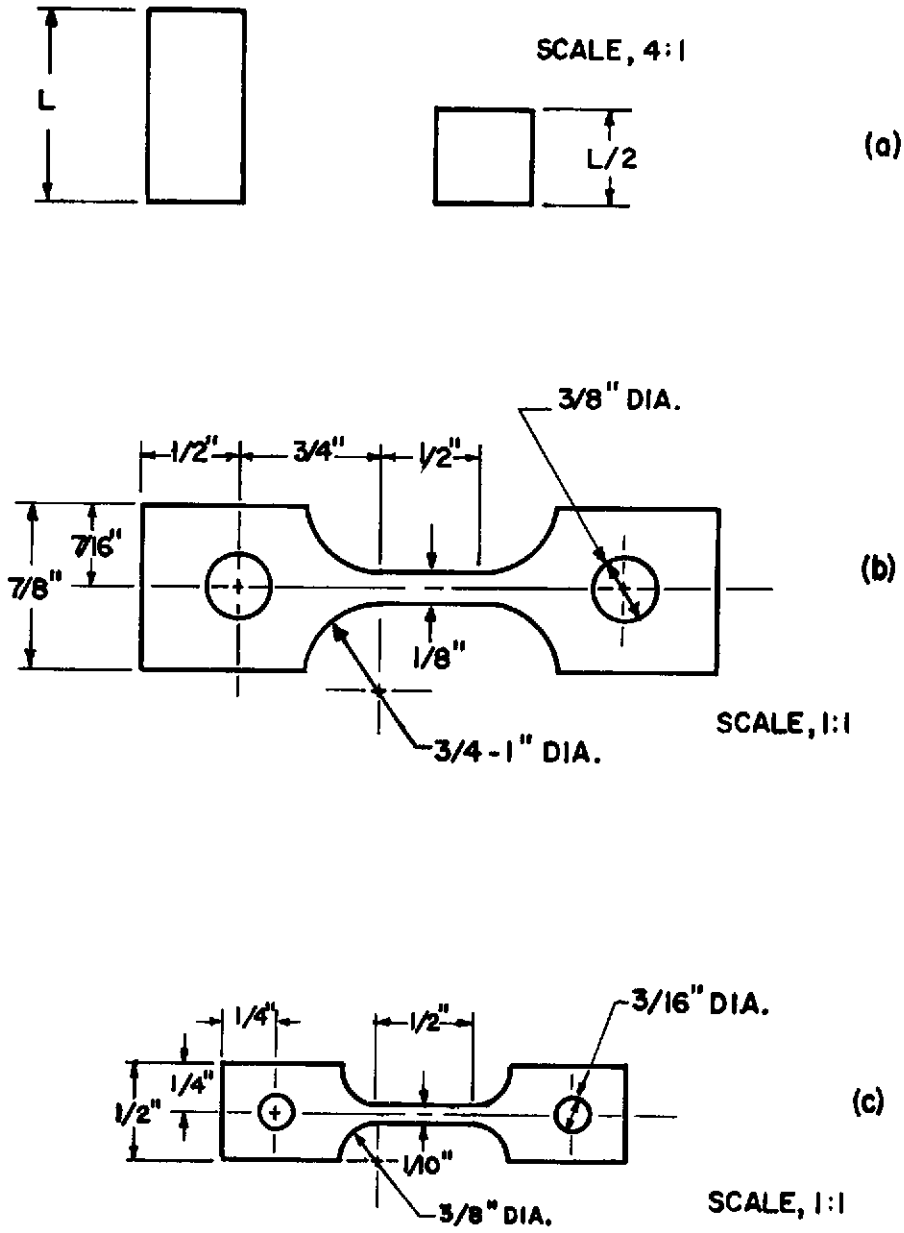

Figure 2 - a) Compression specimen design; b) Tensile specimen design; c) Compact creep specimen for single crystal TD-NiCr.

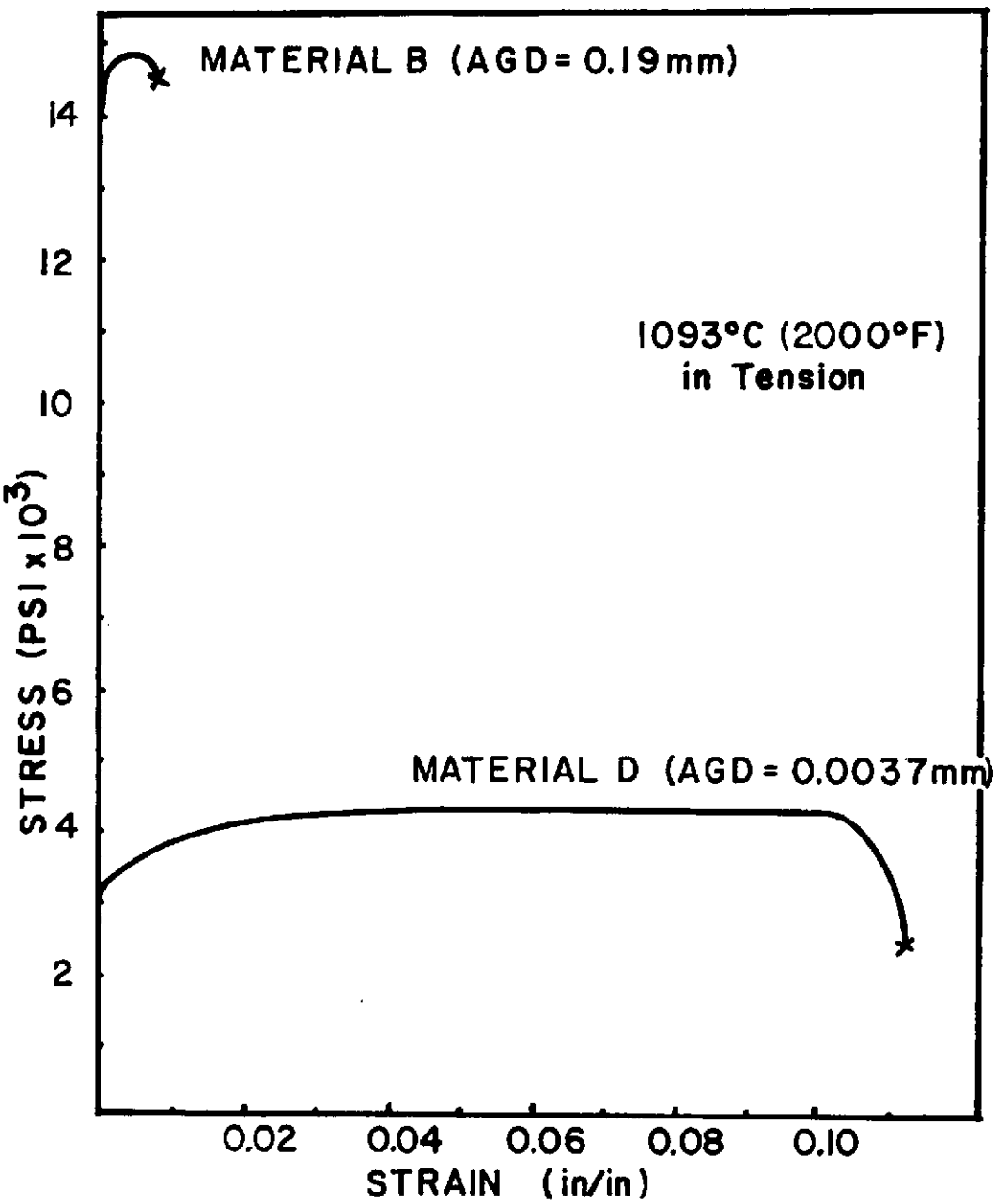

Figure 3 - Stress-Strain curves for Materials B and D at 1093°C (2000°F).

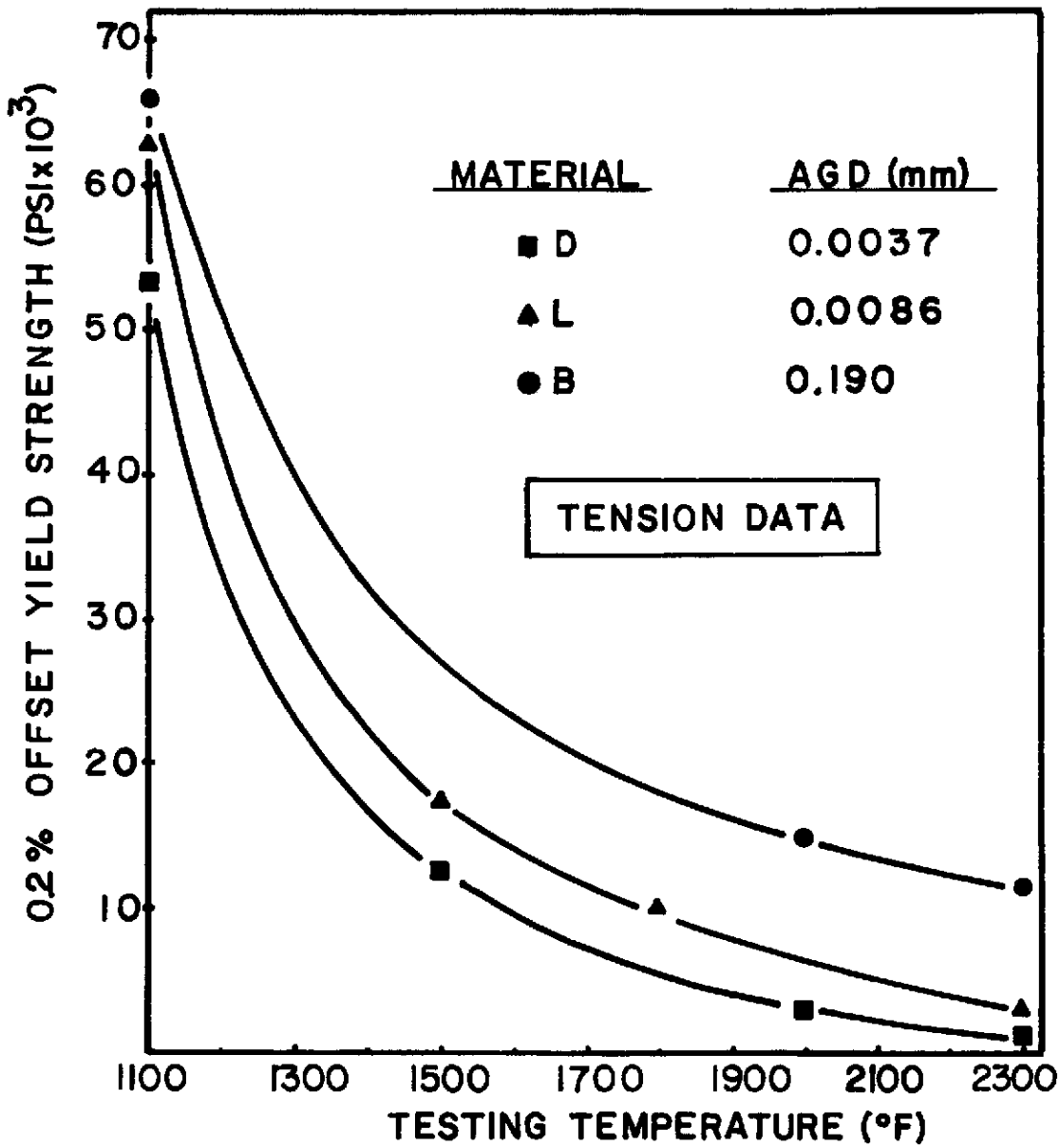

Figure 4 - 0.2 percent offset yield strength of various TD-NiCr materials versus testing temperature (Determined in tension).

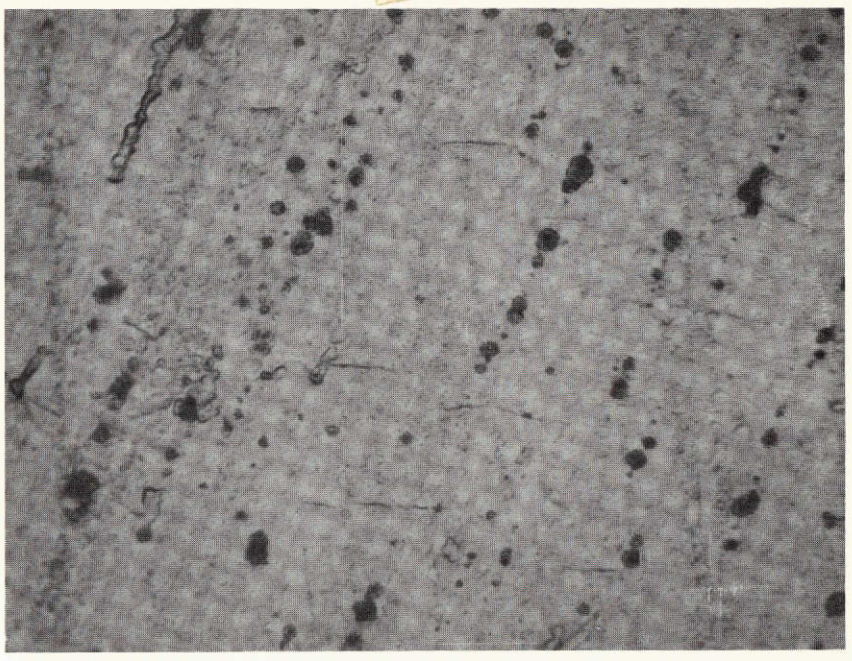

(a) (Side View) (400X)

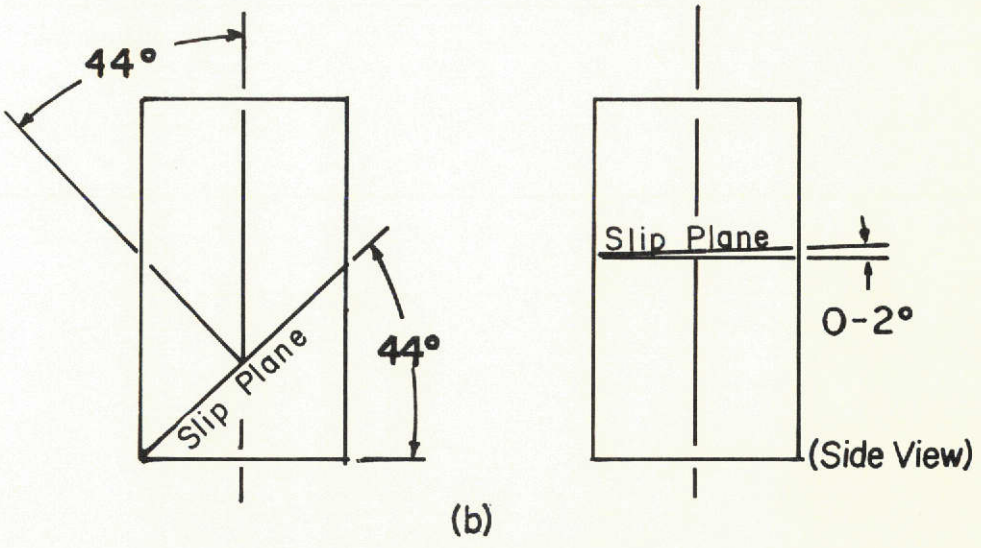

Figure 5 - a) Slip lines on single crystal TD-NiCr compression specimen deformed 3% plastic strain at 1093°C (2000°F); b) orientation of slip plane relative to compression axis.

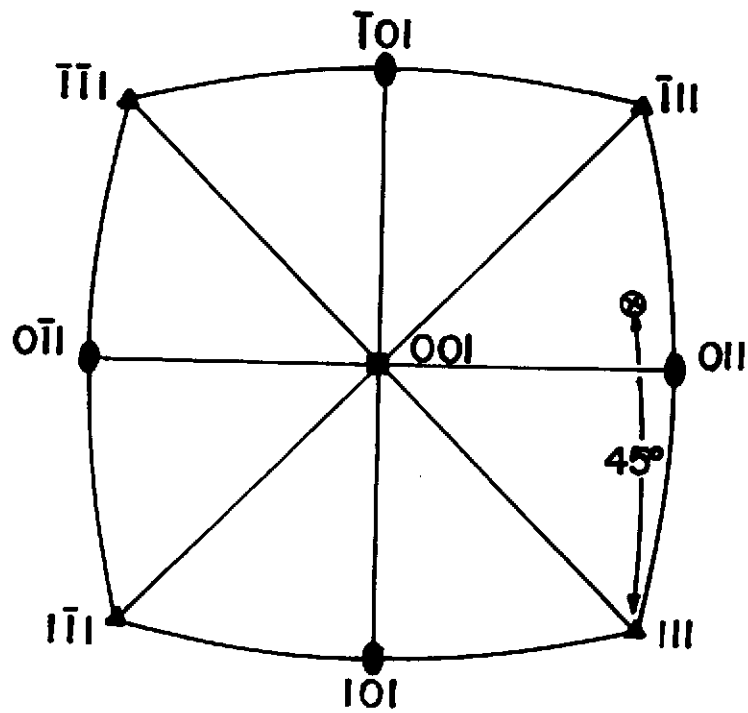

Figure 6 - Standard projection showing orientation of compression axis of specimen (see Figure 5b) relative to slip plane (111).

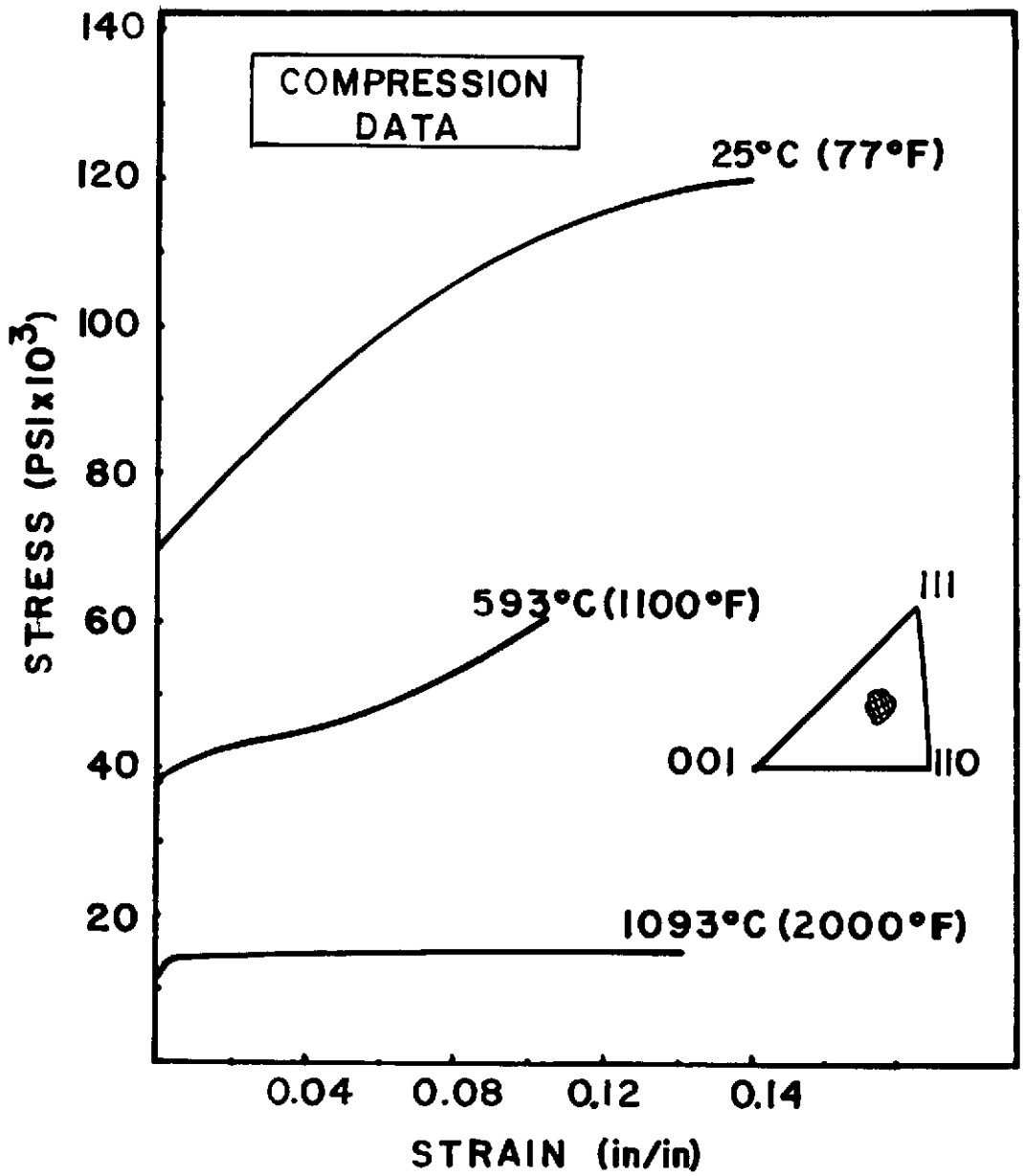

Figure 7 - Stress-Strain curves for single crystal TD-NiCr oriented as shown at various testing temperatures between 25°C (77°F) and 1093°C (2000°F).

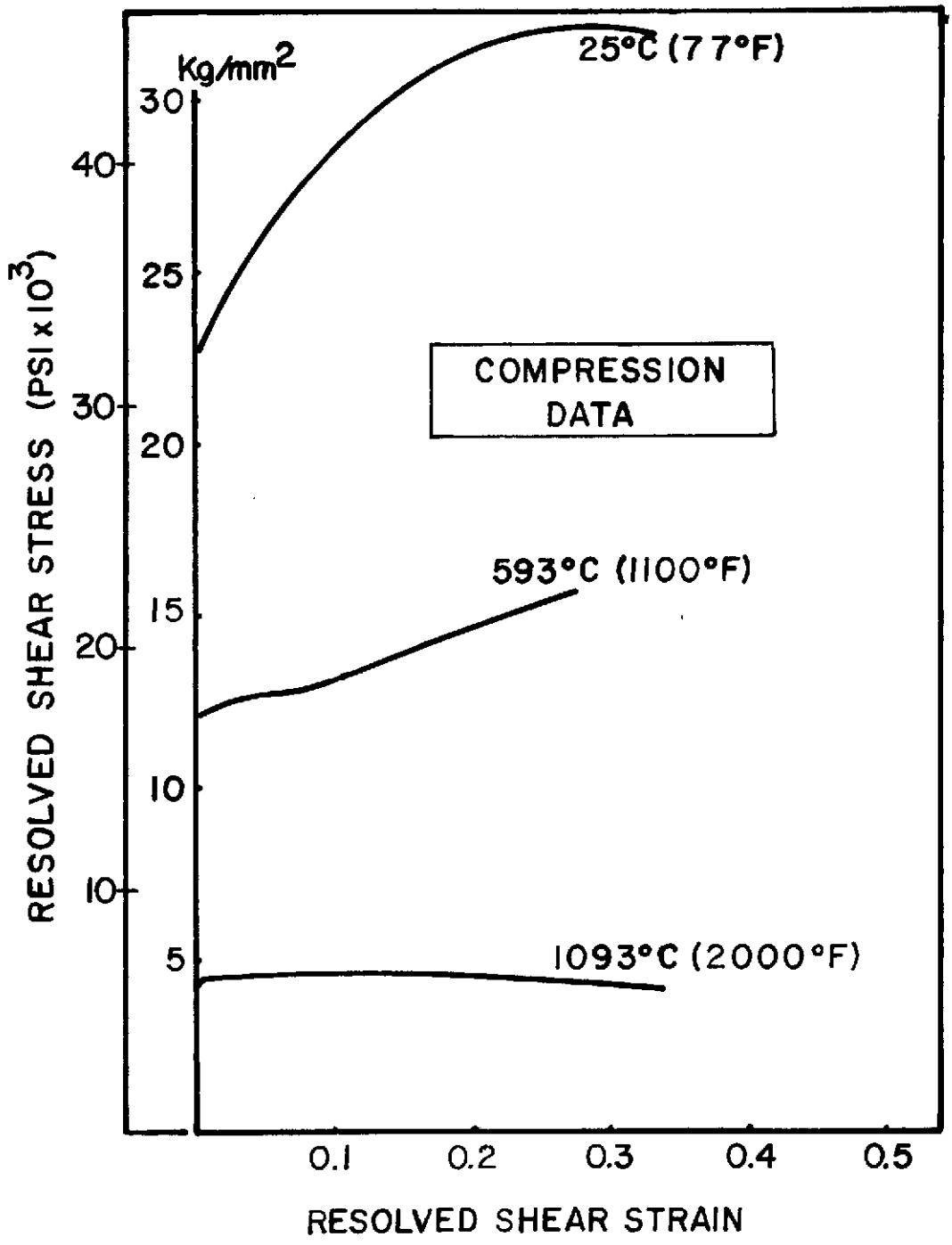

Figure 8 - Shear stress-Shear strain curves of Data in Figure 7.

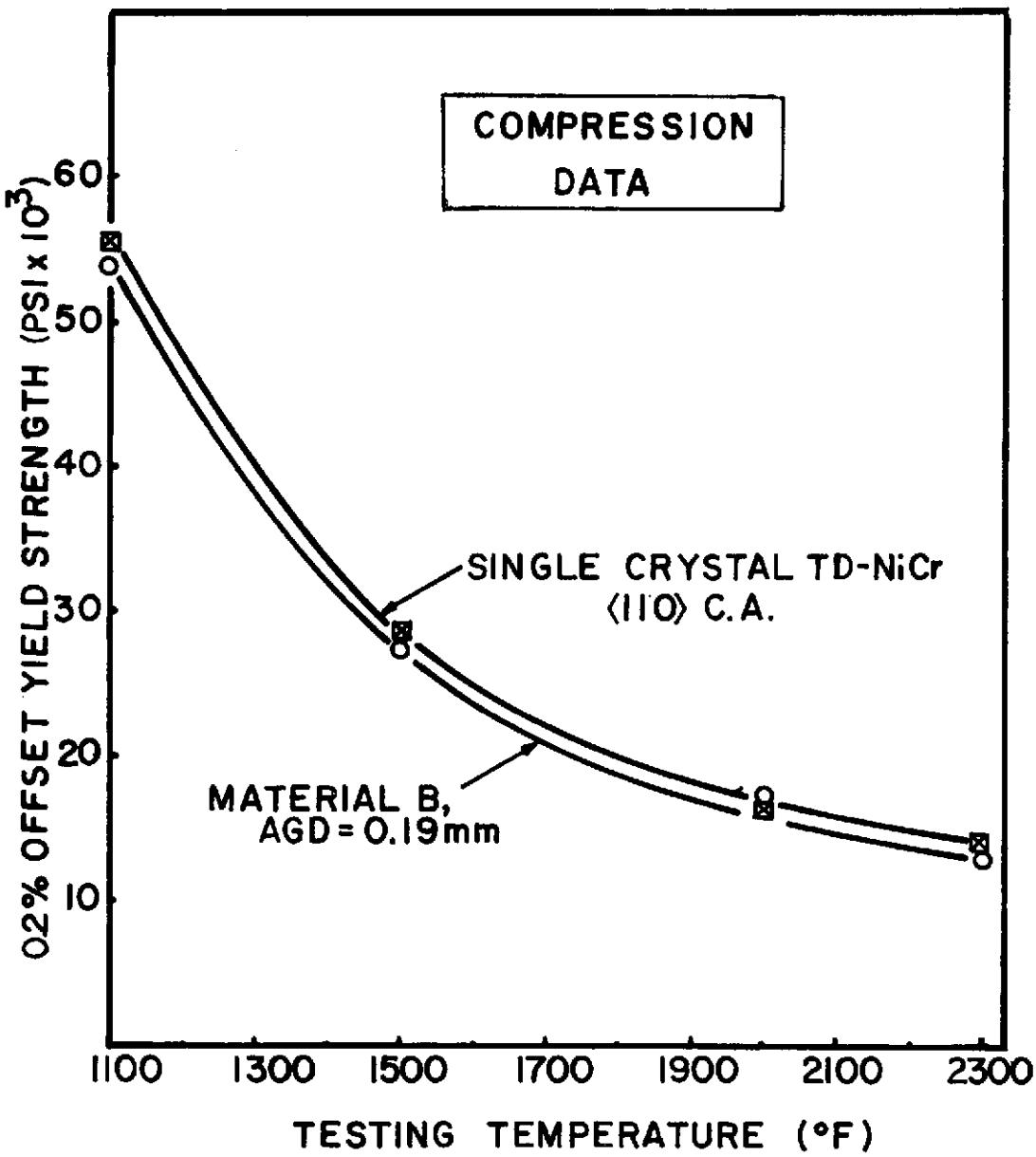

Figure 9 - Comparison of 0.2 percent offset yield strengths for Material B and single crystal 110 versus testing temperature.

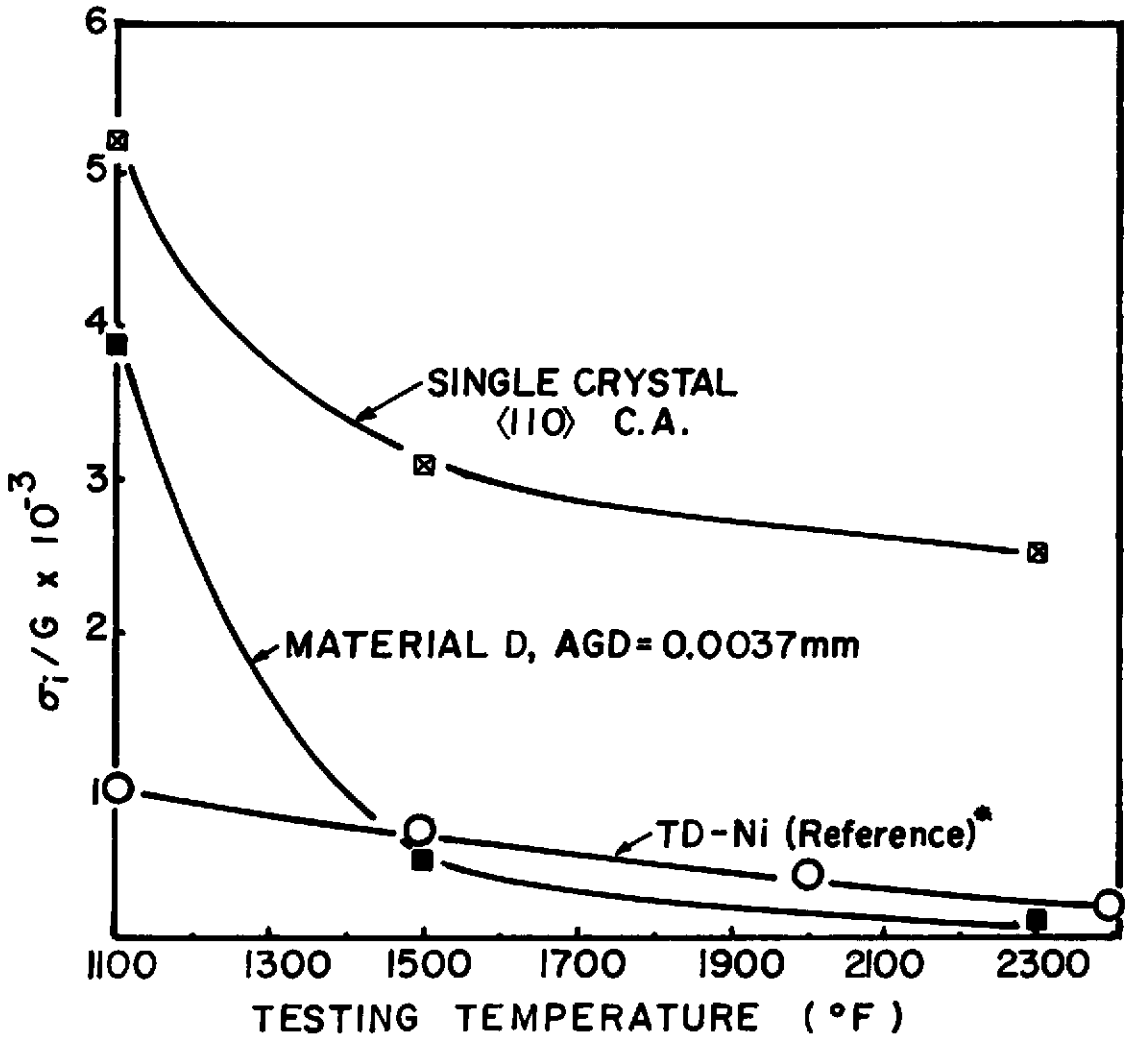

Figure 10 - (Internal stress)/(Shear modulus) versus testing temperature for TD-NiCr (Material D and single crystal) and TD-Nickel (from references 2 and 3).

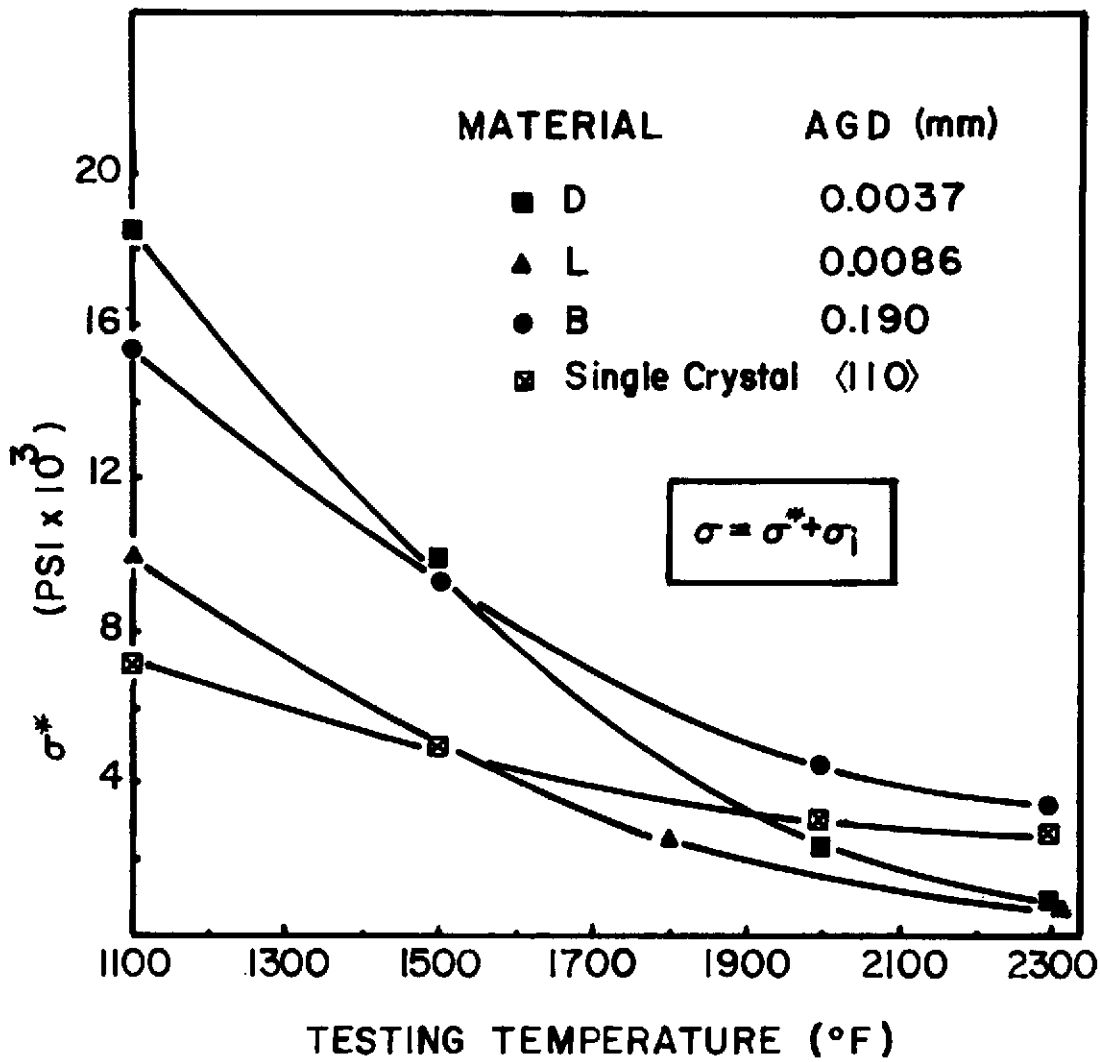

Figure 11 - Effective stress versus testing temperature for various TD-NiCr materials.

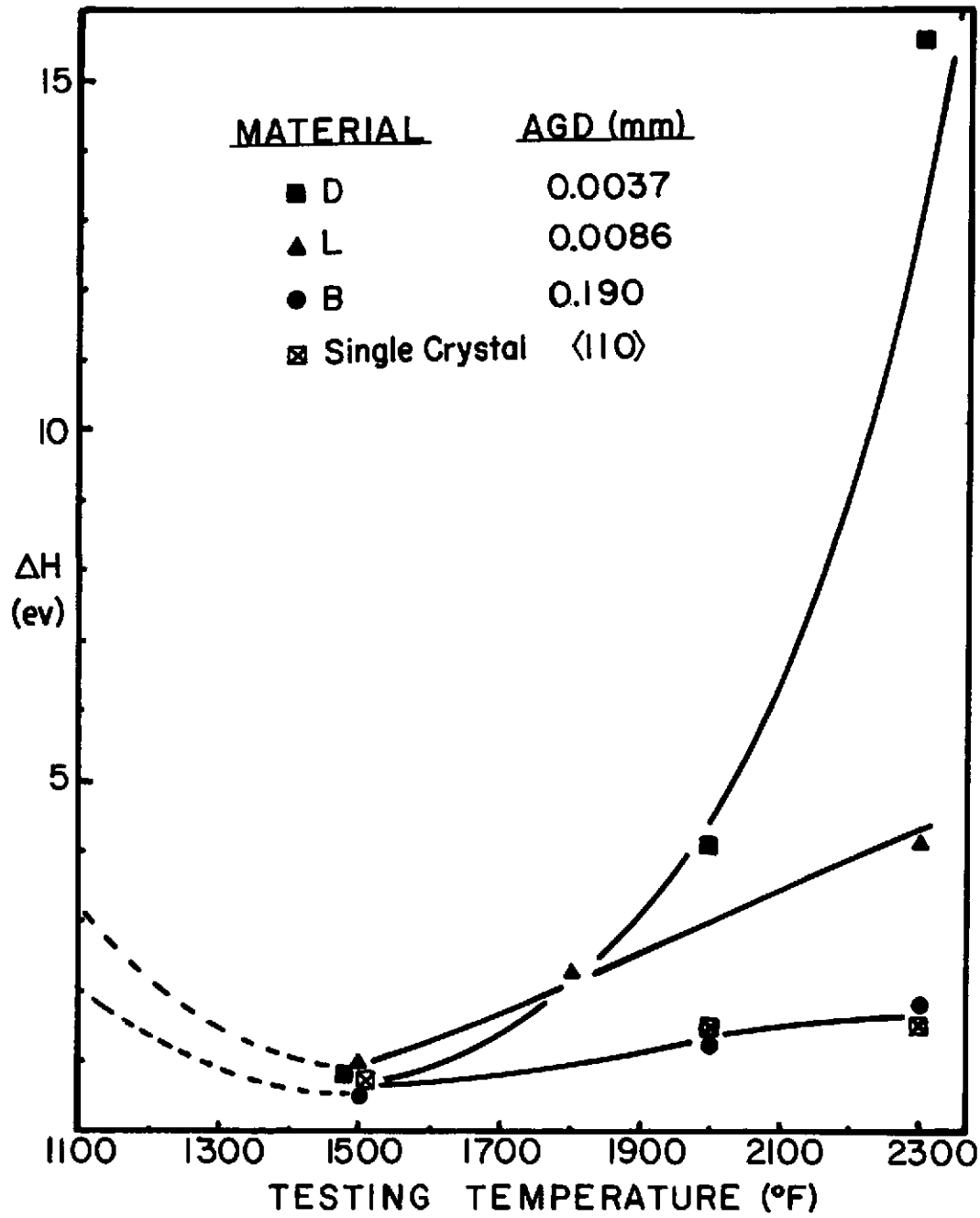

Figure 12 - Activation enthalpy versus testing temperature for various TD-NiCr materials determined in tension and compression.

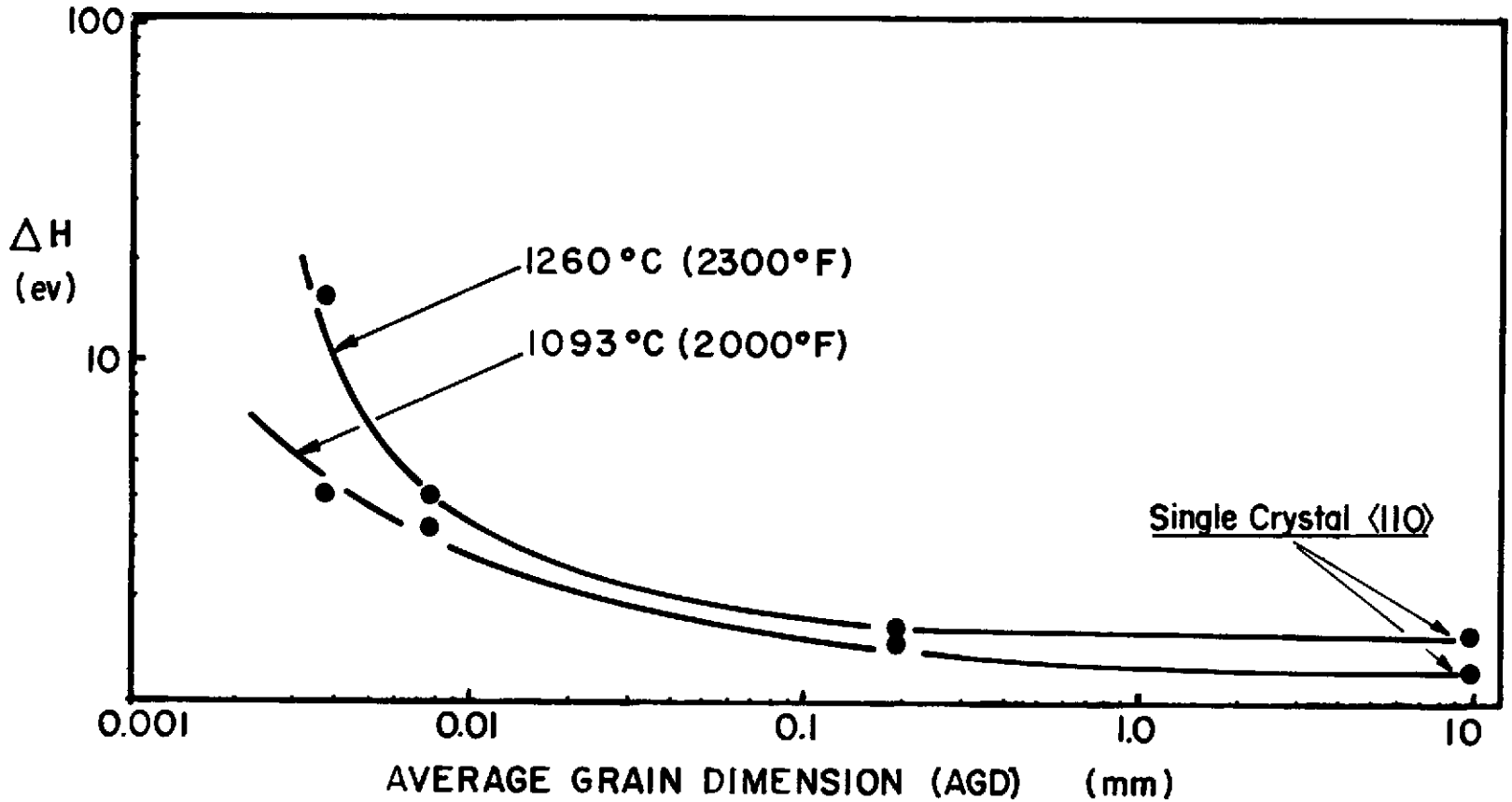

Figure 13 - Activation enthalpy versus grain size for TD-NiCr materials. Values determined in tension and compression at 1093°C (2000°F) and 1260°C (2300°F).

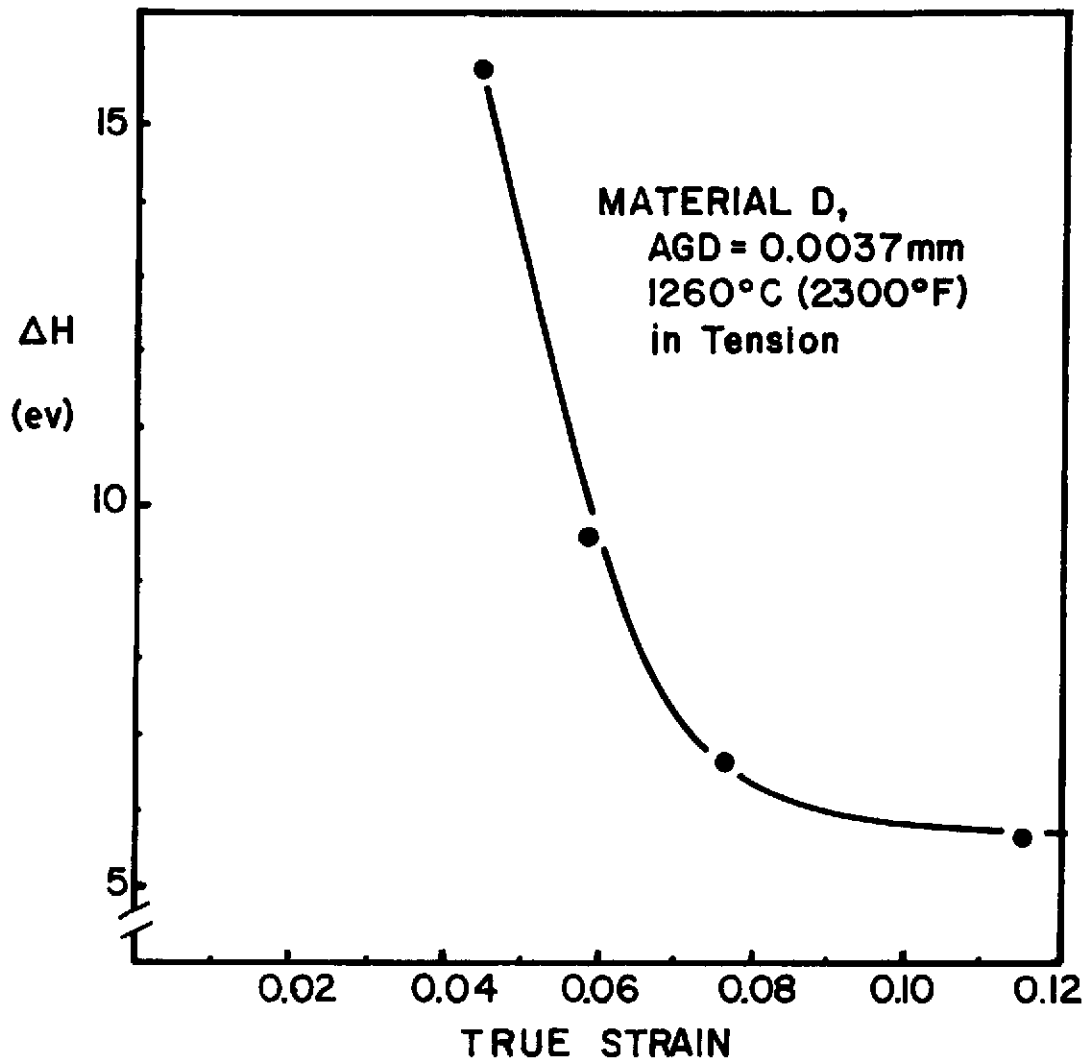

Figure 14 - Activation enthalpy versus true strain for Material D determined in tension at 1260°C (2300°F).

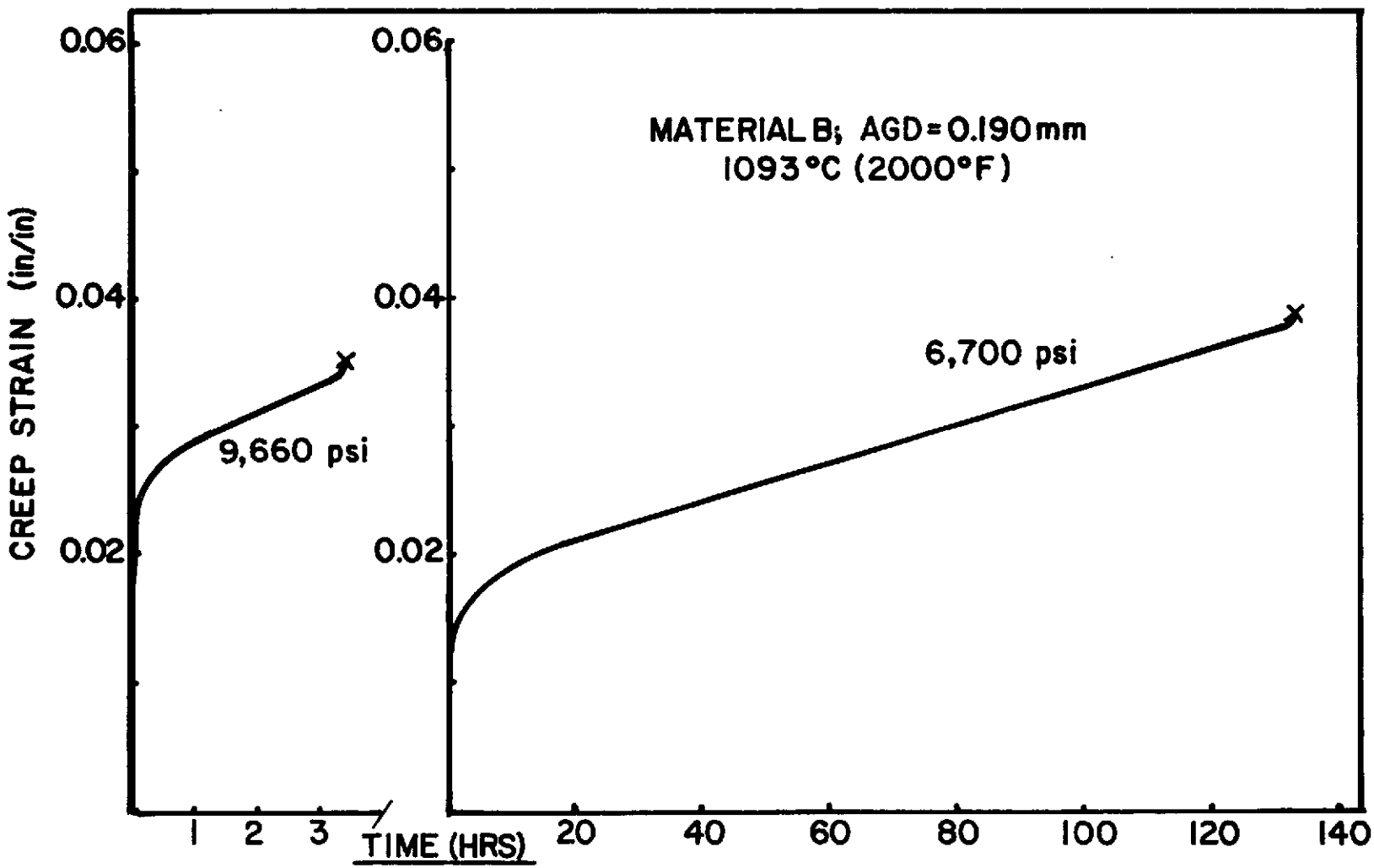

Figure 15 - Conventional creep curves (strain versus time) for Material B at 1093°C (2000°F).

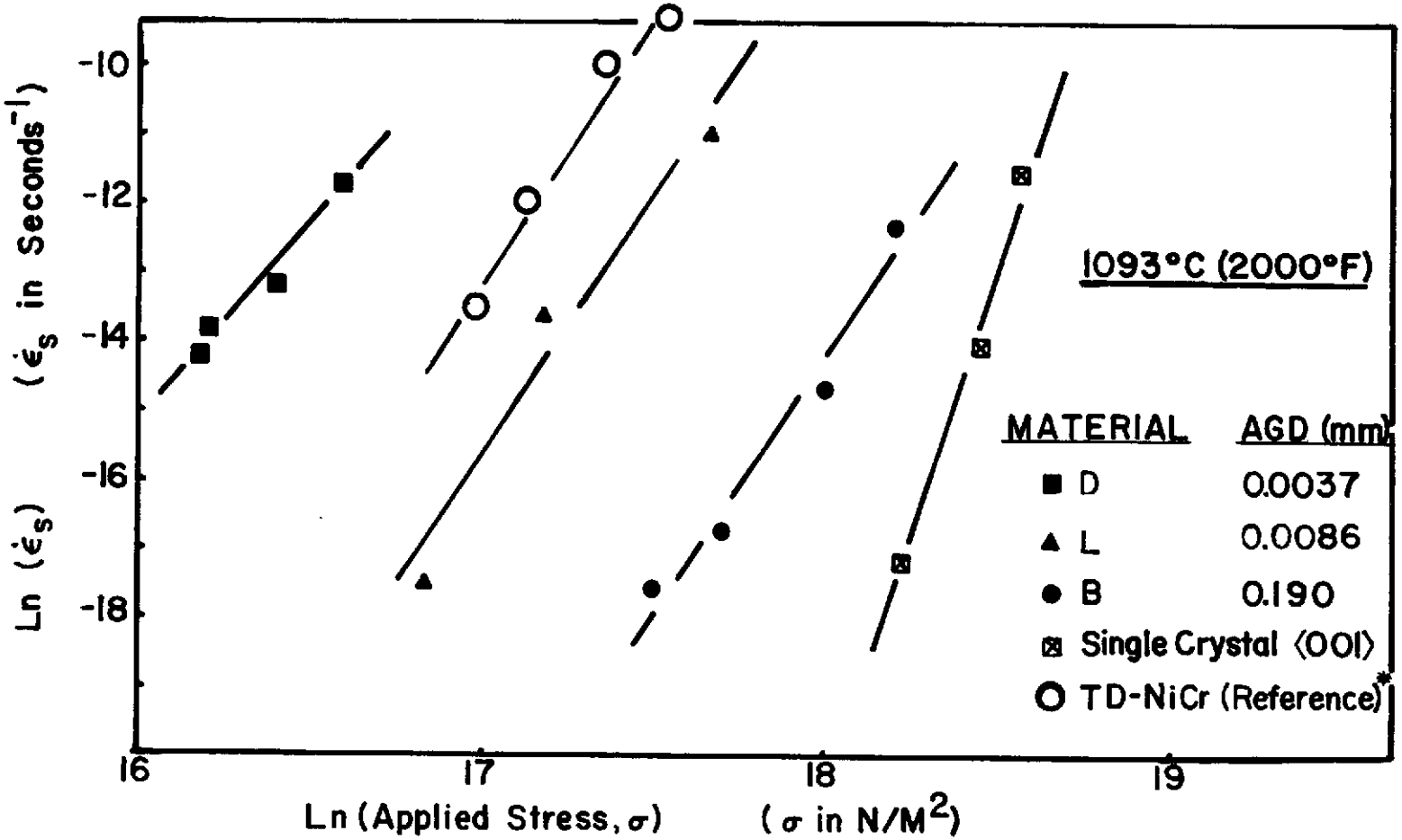

Figure 16 - Ln(Steady state creep rate) versus Ln(Applied stress) for various TD-NiCr materials in creep at 1093°C (2000°F). (Data for TD-NiCr from reference 6 denoted *)

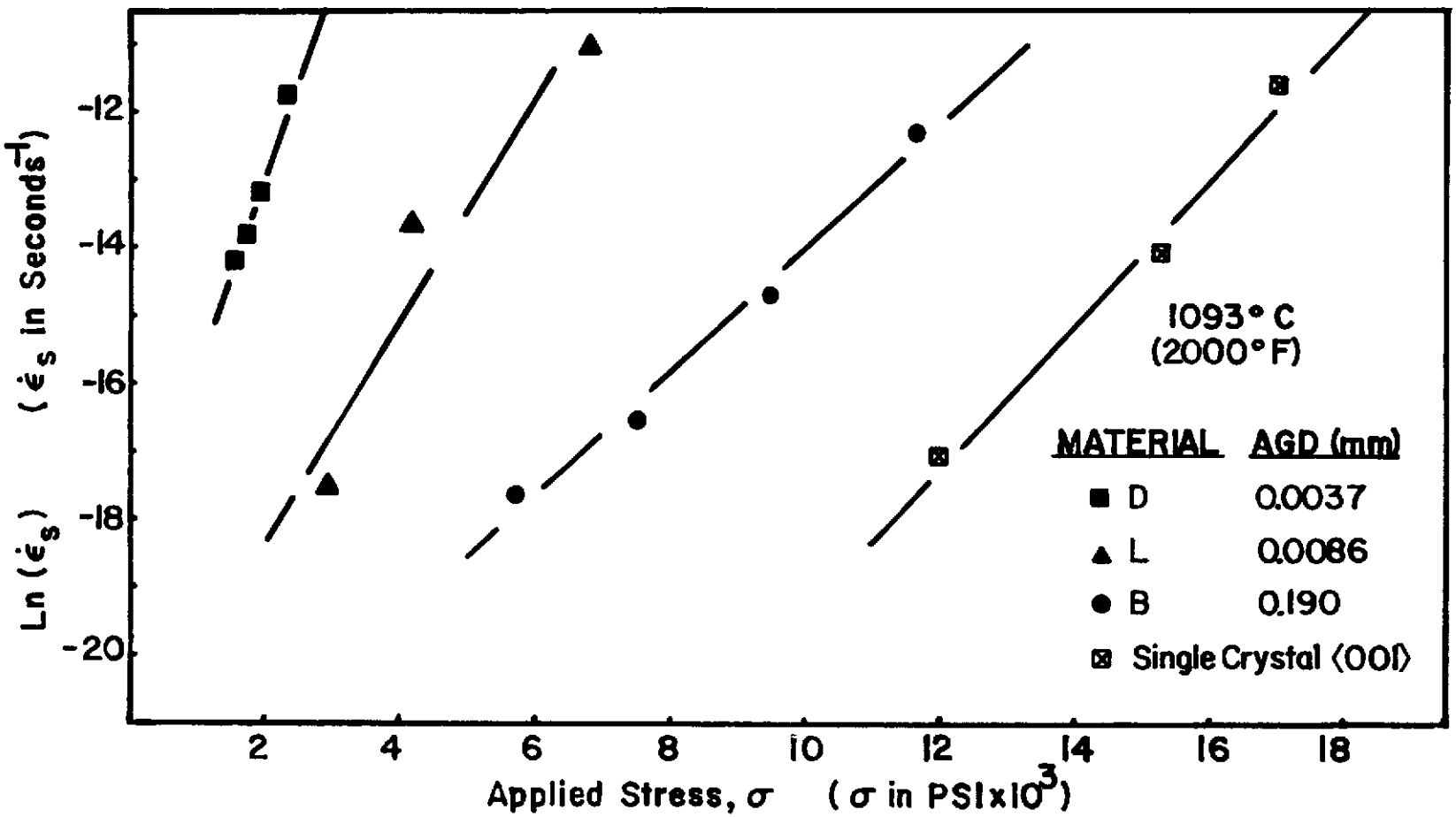

Figure 17 - Ln(Steady state creep rate) versus Applied stress for various TD-NiCr materials in creep at 1093°C (2000°F).

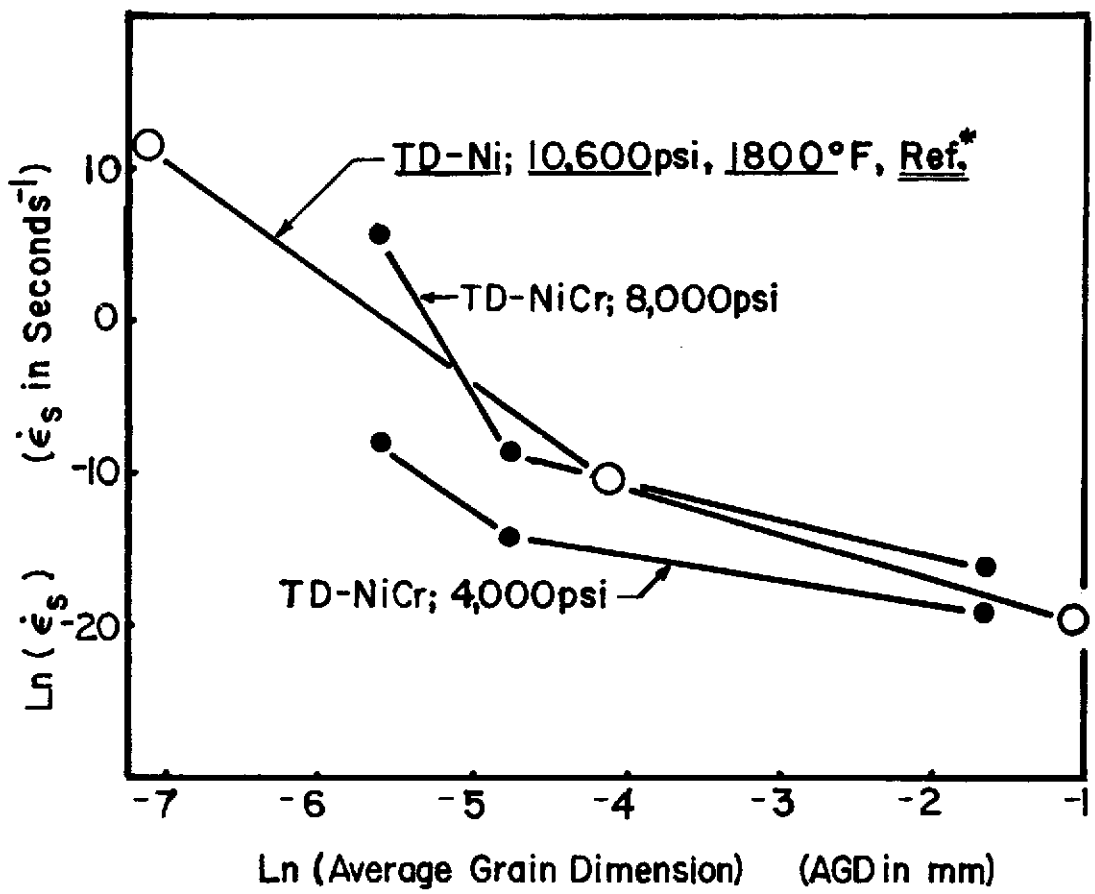

Figure 18 - Ln(Staady state creep rate) versus Ln (Average grain dimension) for varigus TD-NiCr materials in creep at 1093°C (2000°F). Also shown is data for TD-Nickel at 982°C (1800°F).

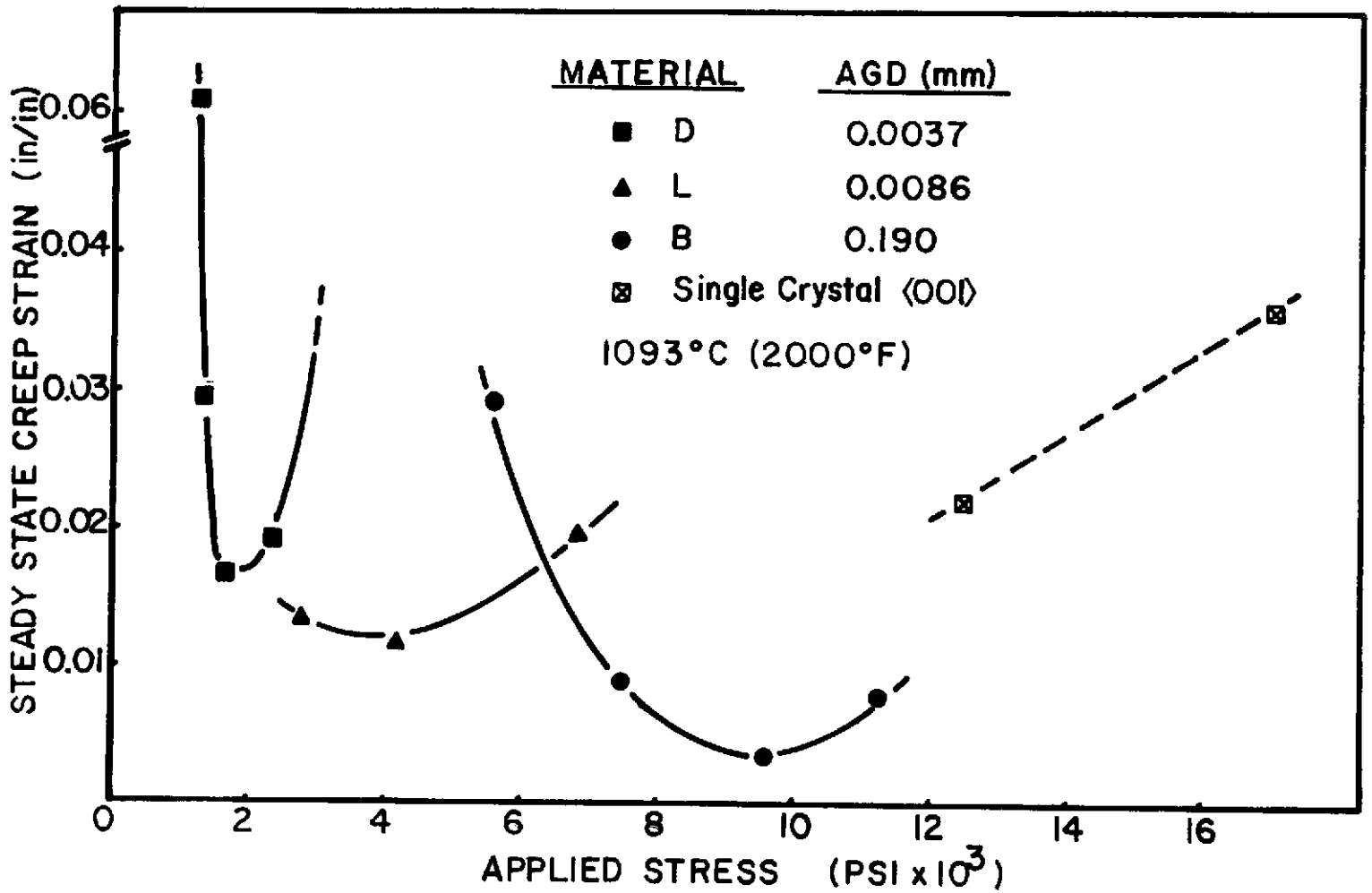

Figure 19 - Steady state creep strain versus Applied stress for TD-NiCr materials in creep at 1093°C (2000°F).

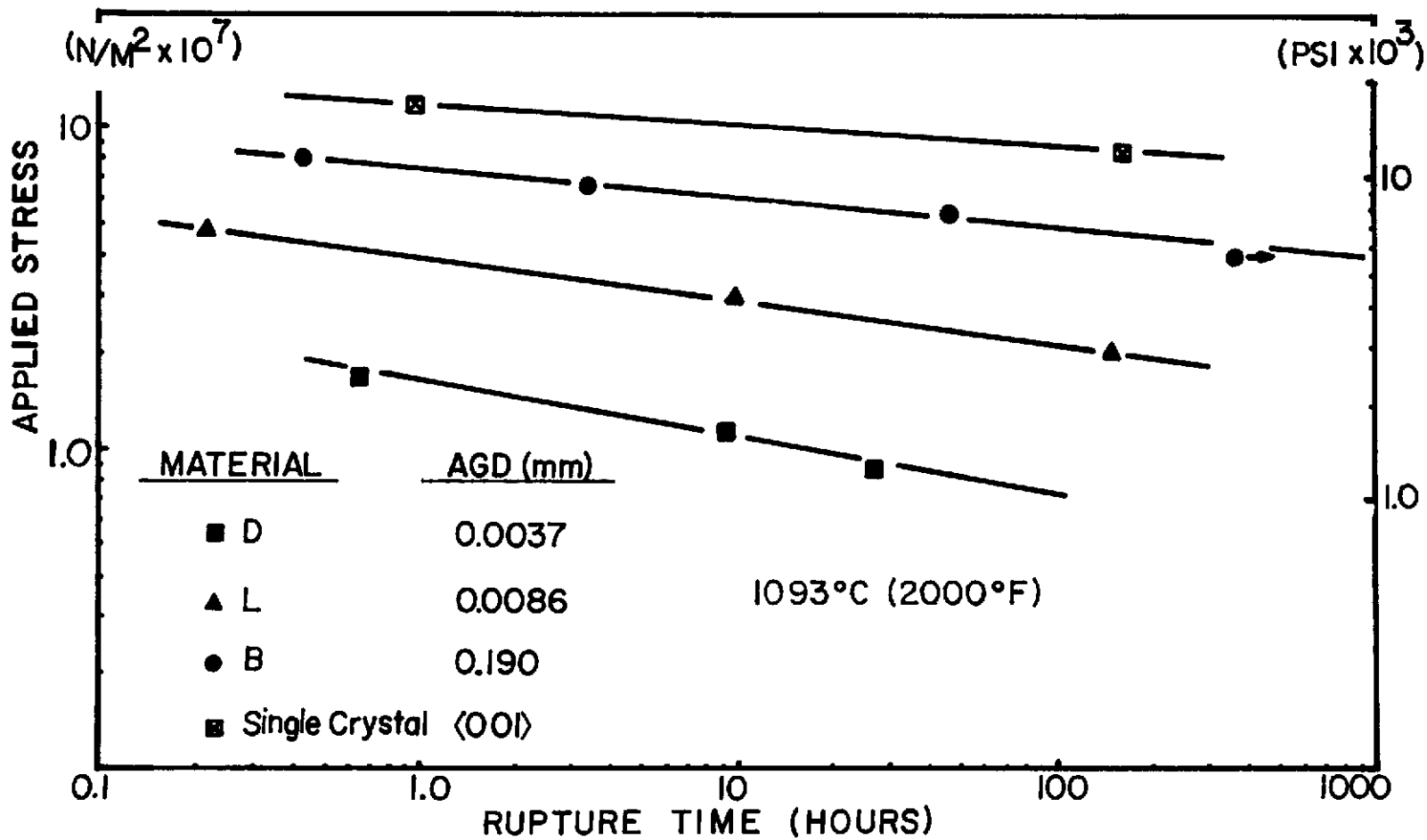

Figure 20 - Applied stress versus Time to failure (Rupture time) for TD-NiCr materials in creep at 1093°C (2000°F).

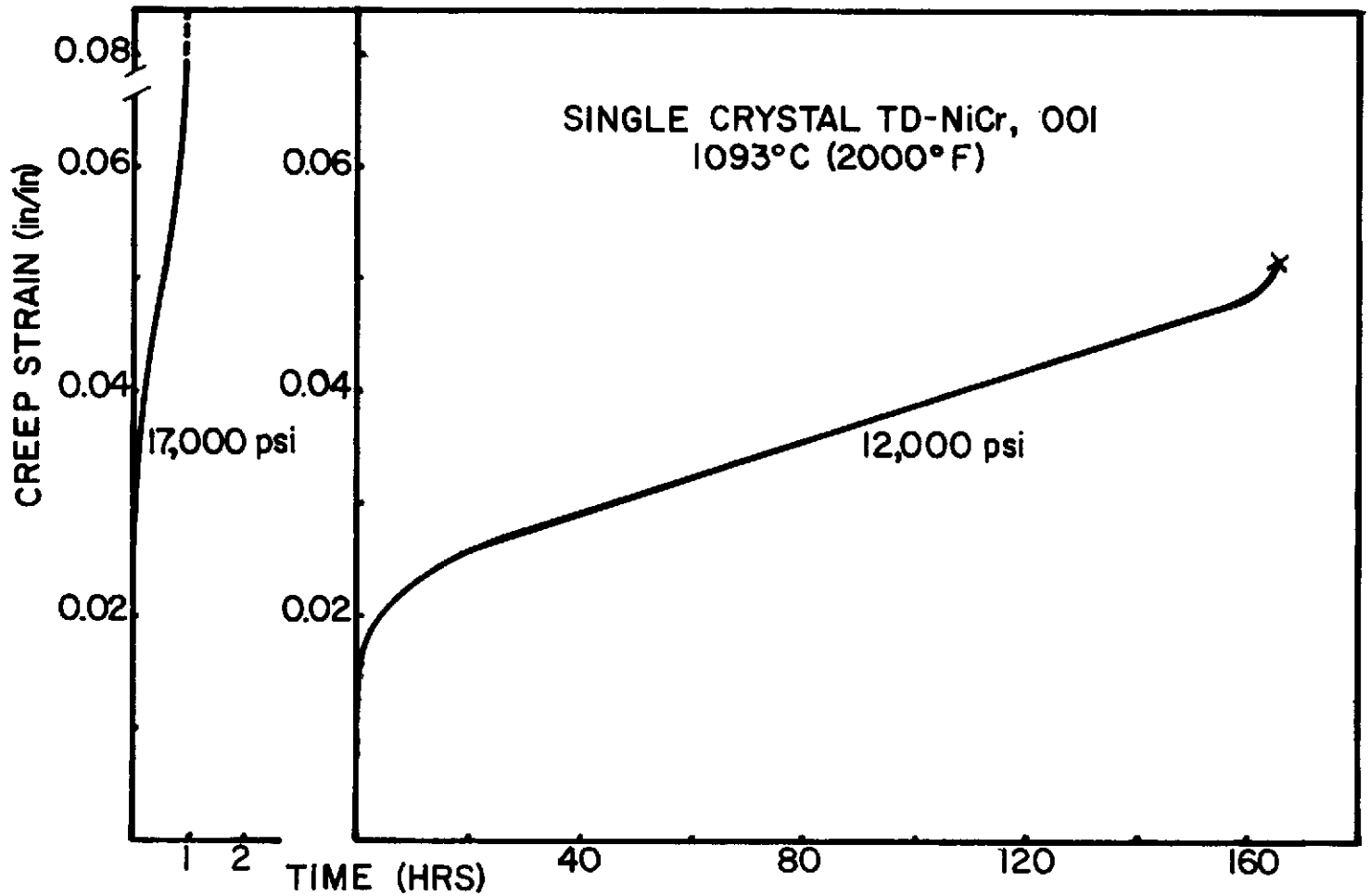

Figure 21 - Conventional creep curves (strain versus time) for 001 TD-NiCr single crystal in creep at 1093°C (2000°F).

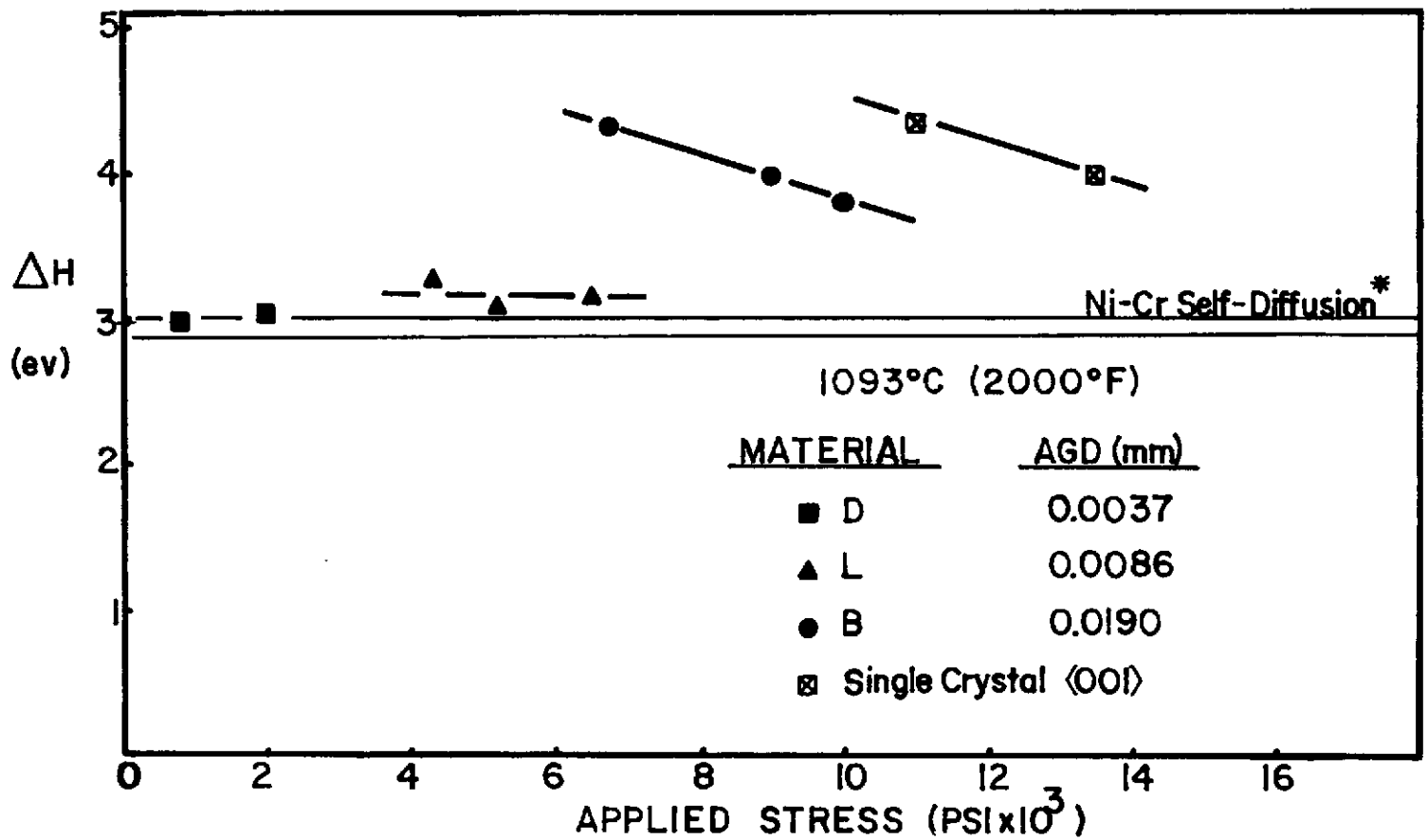

Figure 22 - Activation enthalpy versus Applied stress for TD-NiCr materials. Determined in creep at 1093°C (2000°F).

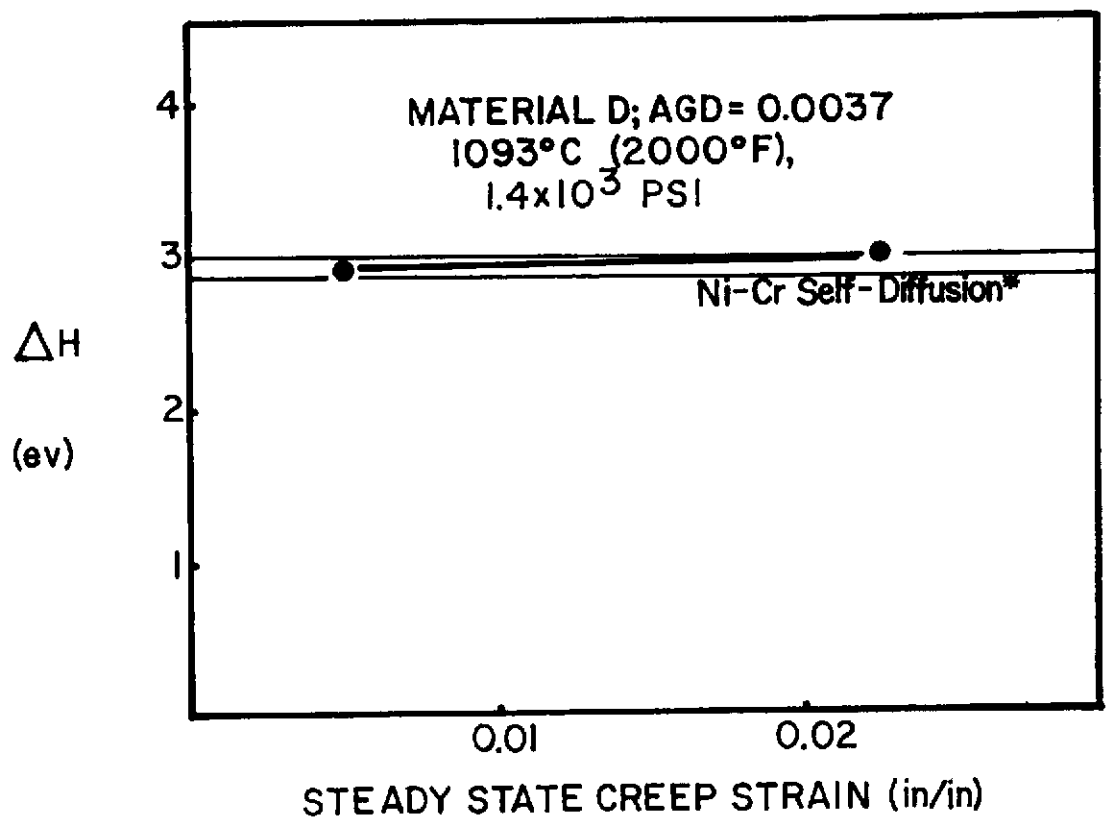

Figure 23 - Activation enthalpy versus Secondary creep strain for Material D determined in creep at 1093°C (2000°F).

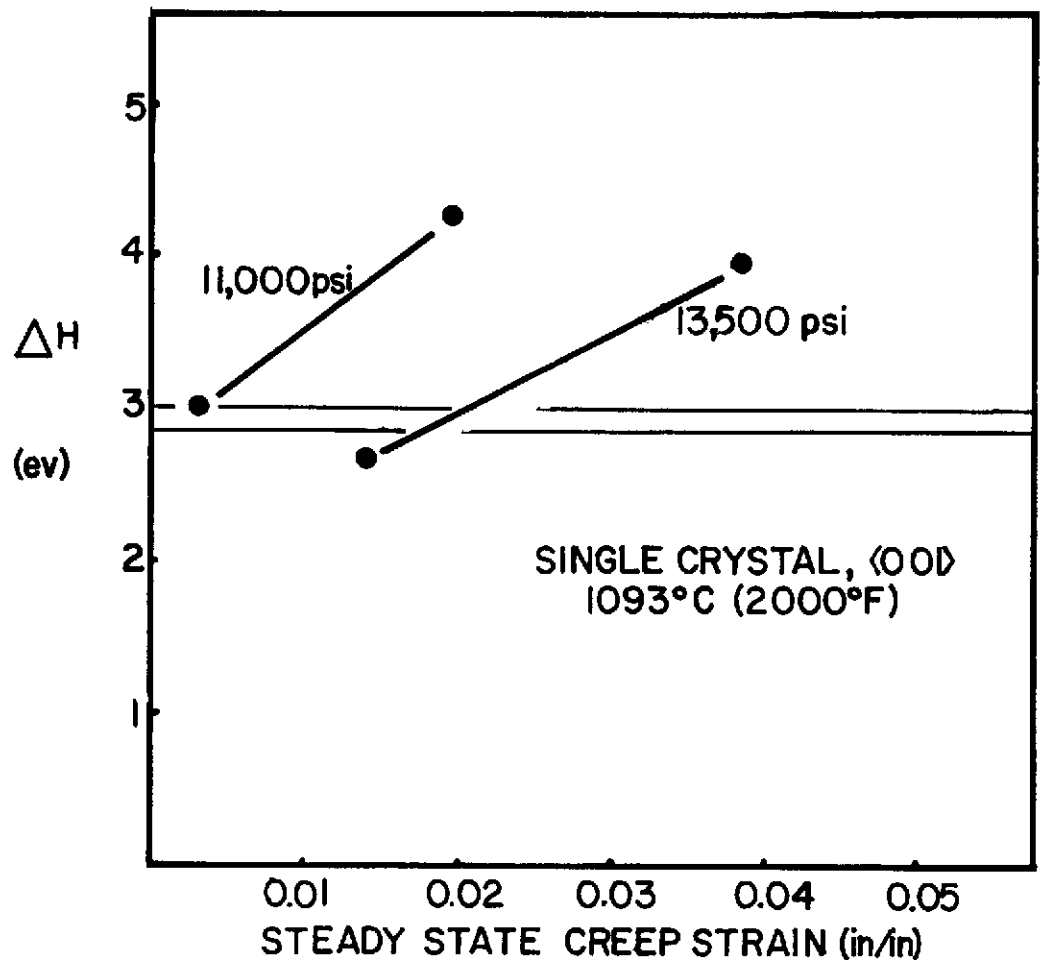

Figure 24 - Activation enthalpy versus Secondary creep strain for 001 TD-NiCr single crystal determined in creep at 1093°C (2000°F).

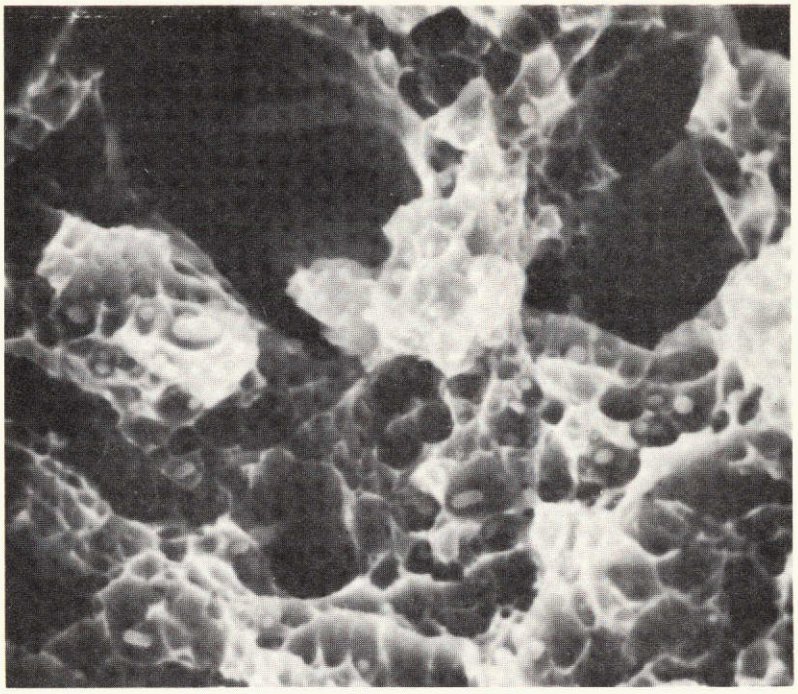

(a)

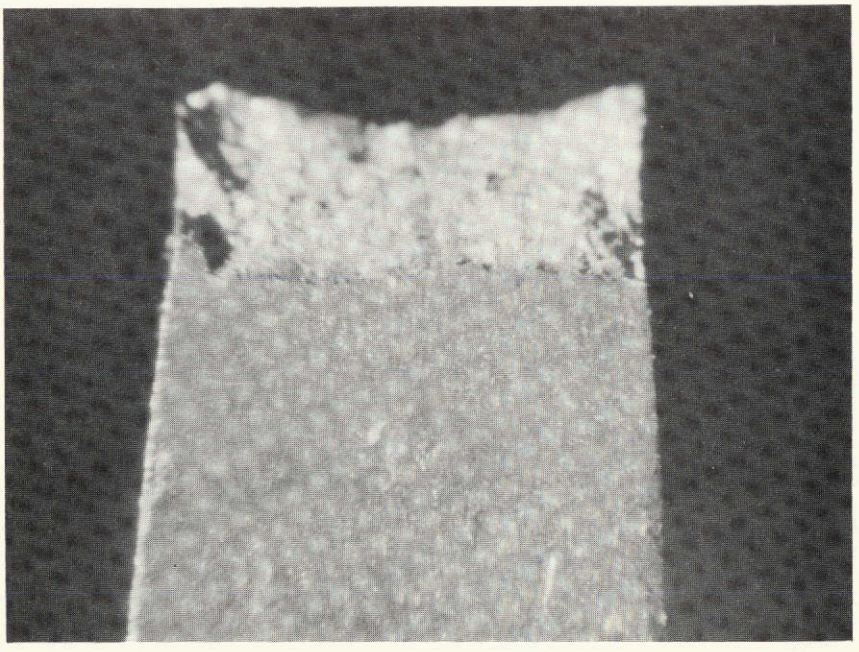

(b)

Figure 25 - a) Scanning Electron Micrograph of Material D deformed in tension at 25°C (77°F),(17,000X) b) Optical micrograph of fracture region (20X).

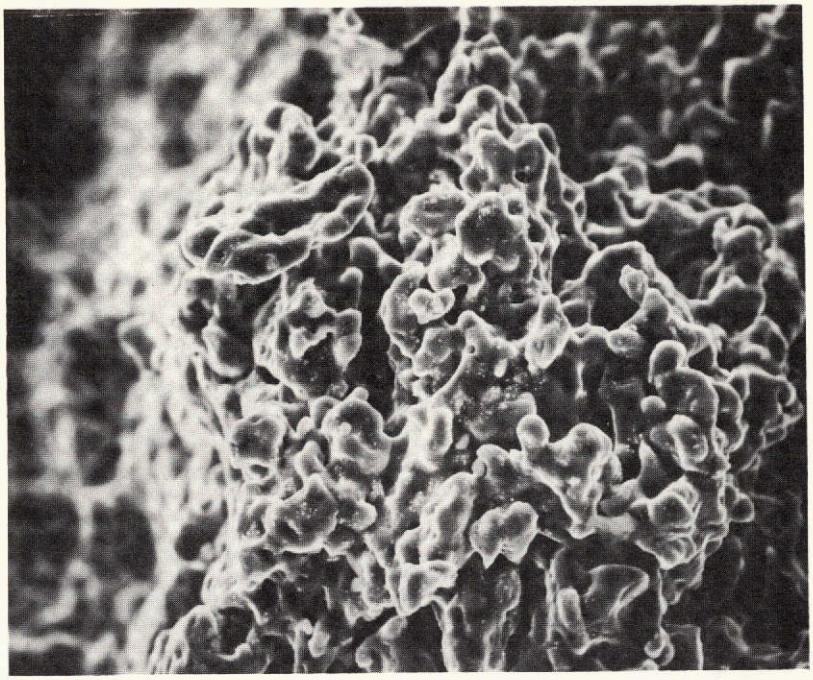

(a)

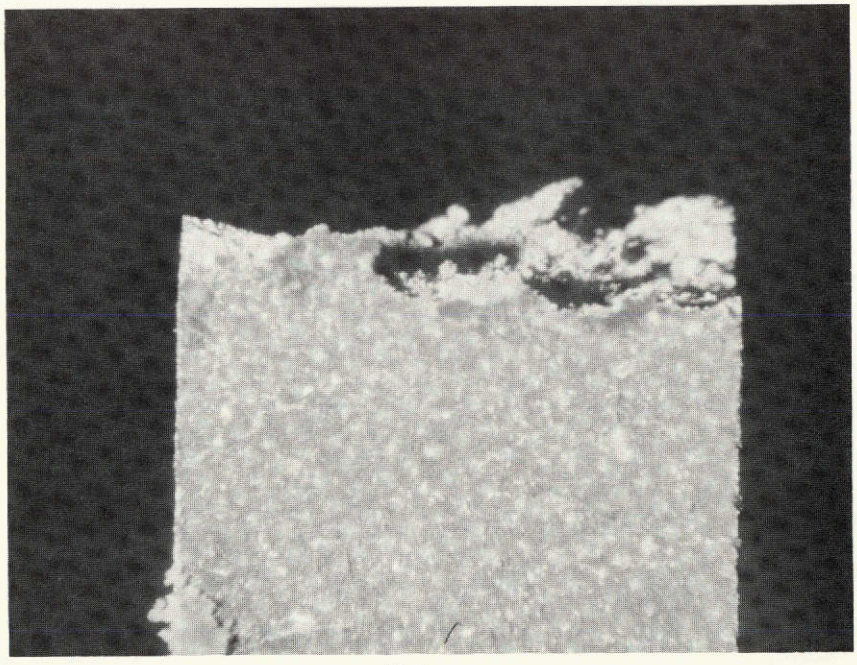

(b)

Figure 26 - a) Scanning Electron Micrograph of Material D deformed in tension at 1093°C (2000°F), (1700X). b) Optical micrograph of fracture region (20X).

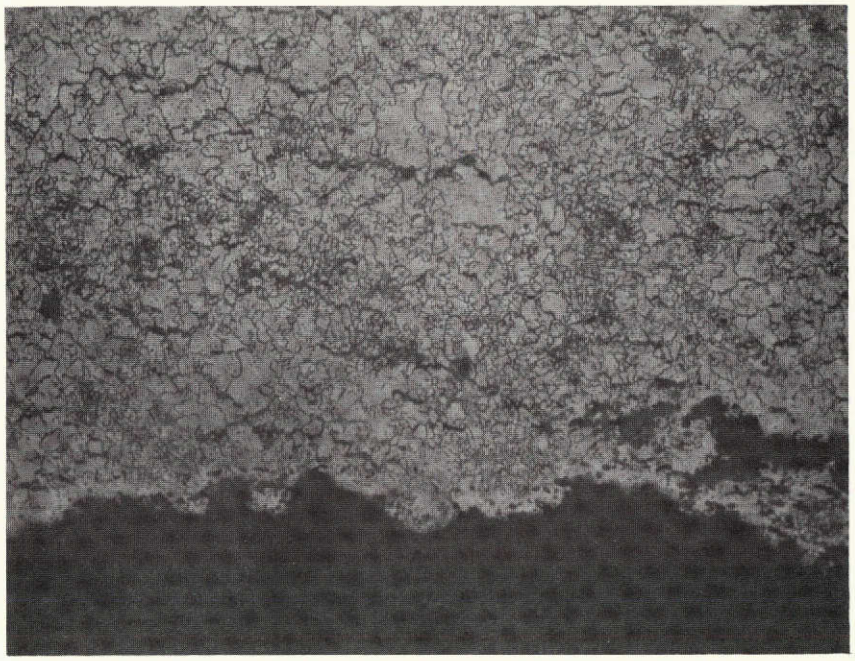

Figure 27 - Optical micrograph of Material (See Figure 26) after tensile fracture at 1093°C (2000°F). Note intergranular cavitation on grain boundaries perpendicular to tensile axis. (Tensile axis vertical)

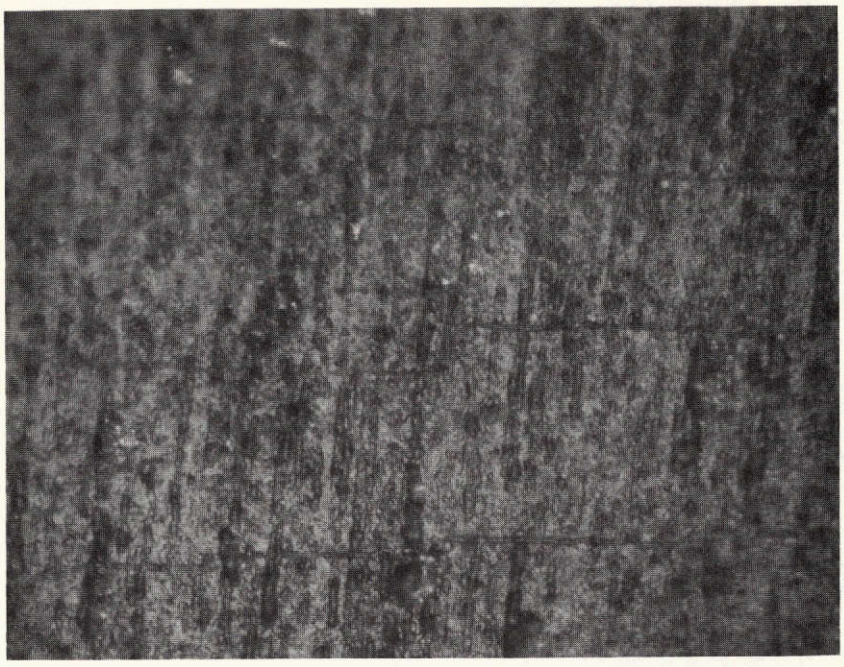

(a)

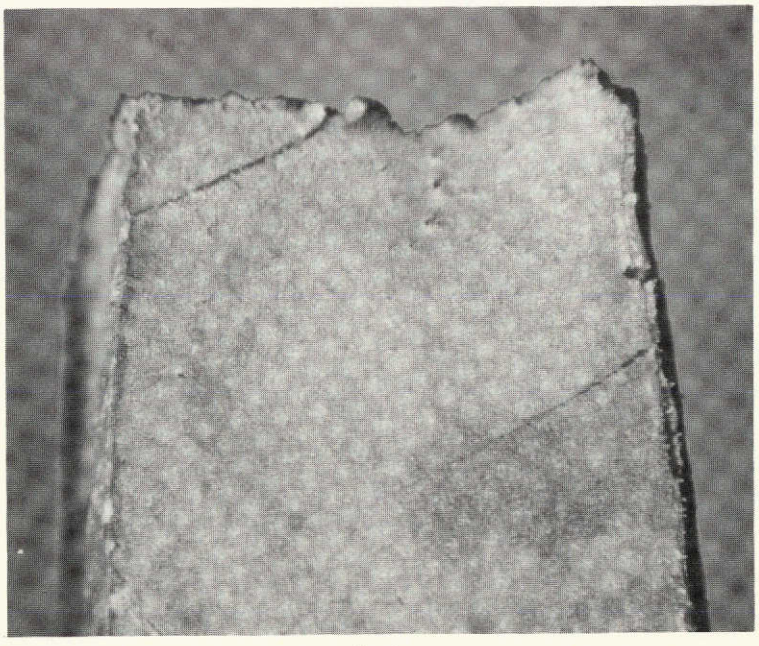

(b)

Figure 28 - a) Surface of 001 TD-NiCr single crystal after creep at 1093°C (2000°F), applied stress 17,000 psi, showing slip line features (horizontal lines)(400X). b) Micrograph of fracture region (30X).

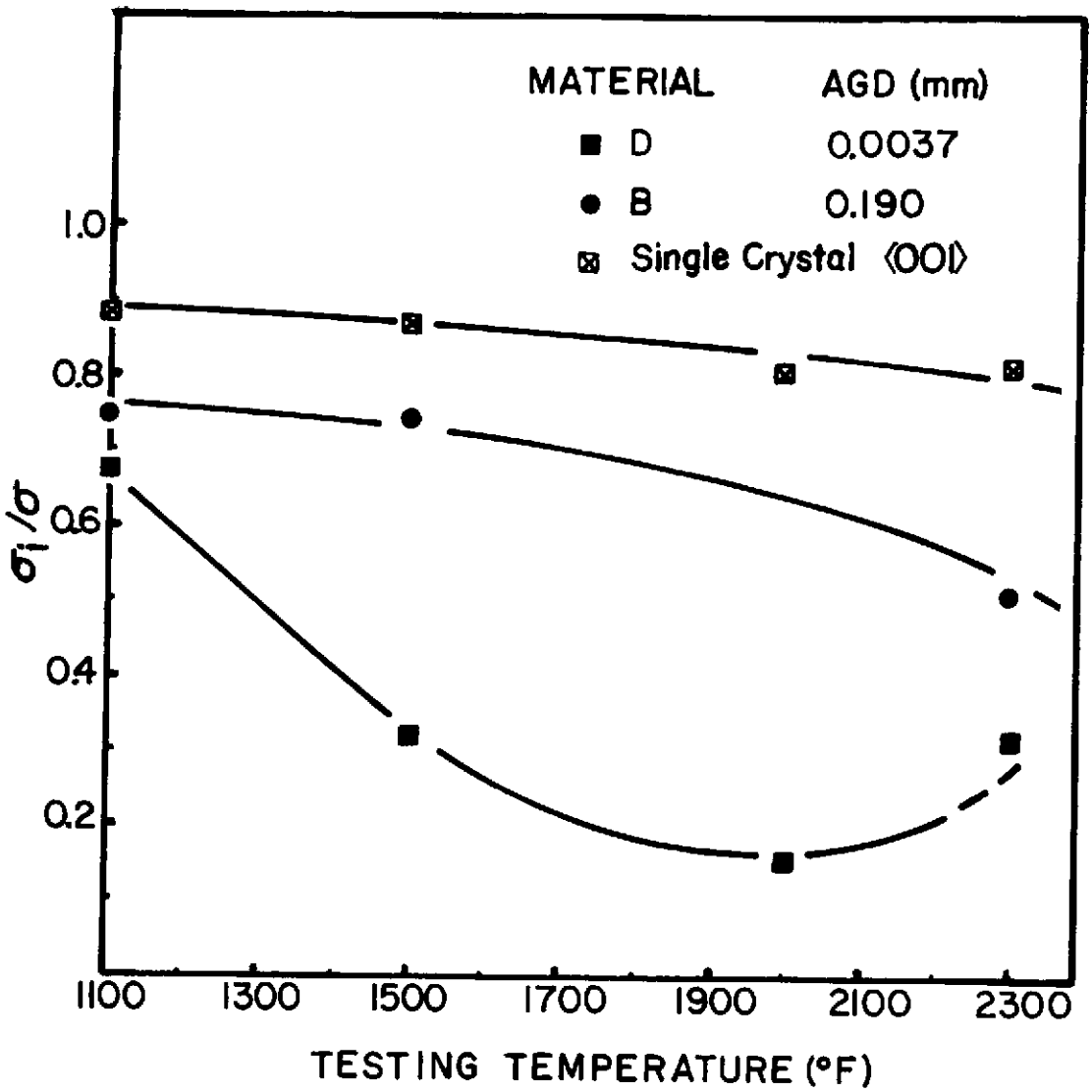

Figure 29 - (Internal Stress)/(Applied stress) versus testing temperature. Determined in tension and compression for various TD-NiCr materials.

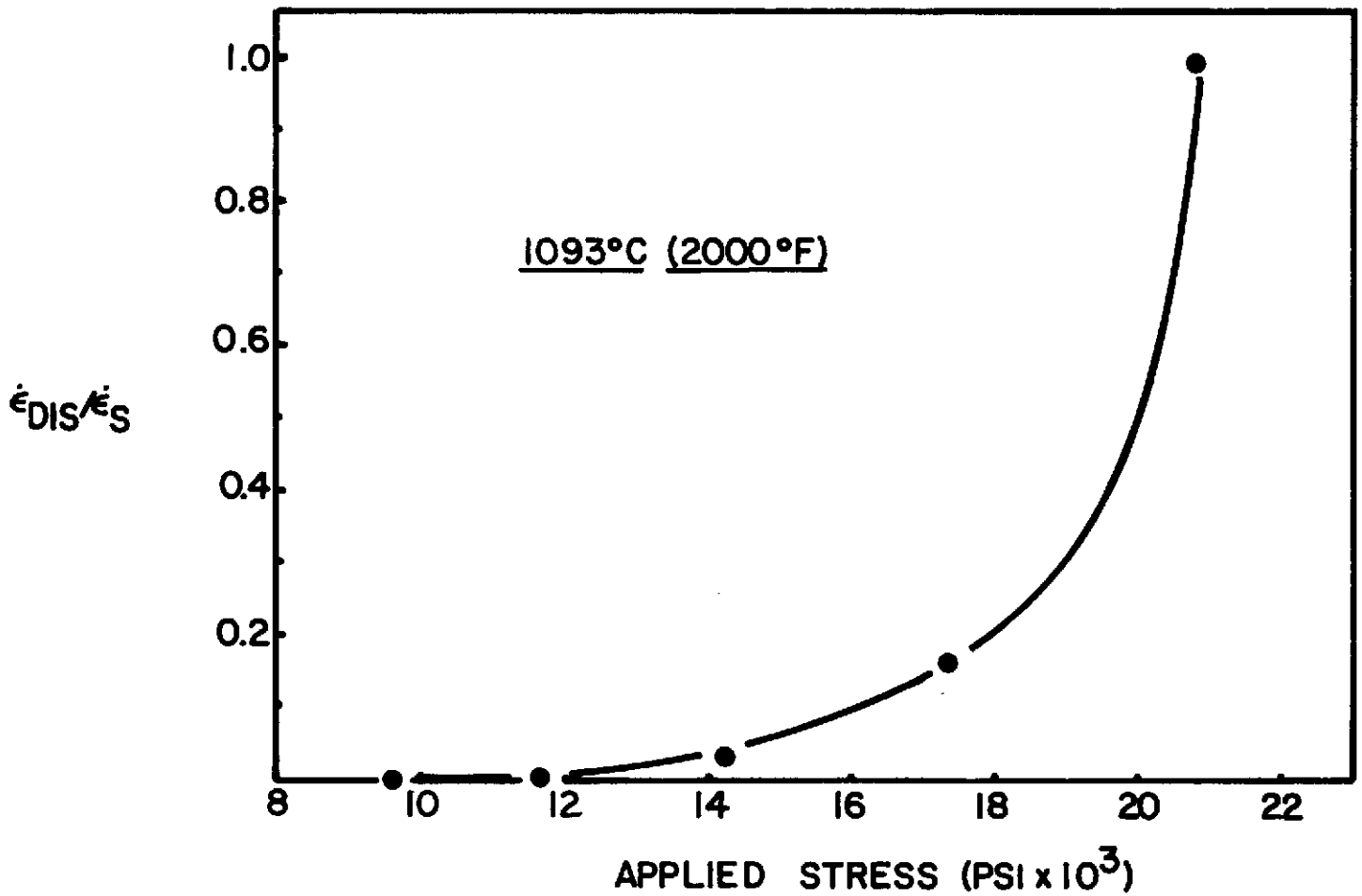

Figure 30 - Estimation of the contribution of dislocation motion in Material B as a function of stress during creep testing at 1093°C (2000°F).